

Article

Multi-Index Approach to Assess and Monitor Meteorological and Agricultural Drought in the Mediterranean Region: Case of the Upper Oum Er Rabia Watershed, Morocco

Mohammed Mouad Mliyah ¹, Yassine Ait Brahim ², Eleni-Ioanna Koutsovili ³, Ourania Tzoraki ⁴,
Ahmed Zian ⁵, Mourad Aqnouy ⁶ and Lahcen Benaabidate ^{1,*}

- ¹ Laboratory of Functional Ecology and Environment Engineering, Faculty of Sciences and Techniques, Sidi Mohammed Ben Abdellah University, Fez 30000, Morocco; mohammedmouad.mliyah@usmba.ac.ma
 - ² International Water Research Institute, University Mohammed VI Polytechnic, Benguerir 43150, Morocco; yassine.aitbrahim@um6p.ma
 - ³ Institute of Crop Science, Scuola Superiore Sant'Anna, 56010 Pisa, Italy; elenioanna.koutsovili@santannapisa.it
 - ⁴ Department of Marine Sciences, School of the Environment, University of the Aegean, 81100 Mytilene, Greece; rania.tzoraki@aegean.gr
 - ⁵ Laboratory of Engineering Sciences and Applications, National School of Applied Sciences, Al Hoceima 32003, Morocco; zian_fr2005@yahoo.fr
 - ⁶ Applied Geology Research Laboratory—AGRSRT, Department of Geosciences, Faculty of Sciences and Techniques, Moulay Ismail University of Meknes, Errachidia 52000, Morocco; mourad.aqnouy@gmail.com
- * Correspondence: lahcen.benaabidate@usmba.ac.ma; Tel.: +212-535608014

Abstract: Drought is a severe disaster, increasingly exacerbated by climate change, and poses significant challenges worldwide, particularly in arid and semi-arid regions like Morocco. This study aims to assess and monitor drought using a multi-index approach to provide a comprehensive understanding of its spatio-temporal dynamics at both meteorological and agricultural levels. The research focuses on the Upper Oum Er Rabia watershed, which spans 35,000 km² and contributes approximately a quarter of Morocco's renewable water resources. We propose a methodology that combines ERA5 temperature data from remote sensing with ground-based precipitation data to analyze drought characteristics. Three meteorological indices were utilized: the Standardized Precipitation Index (SPI), the Standardized Precipitation Evapotranspiration Index (SPEI), and the Reconnaissance Drought Index (RDI). Additionally, three remote-sensing indices were employed to capture agricultural drought: the Normalized Difference Vegetation Index (NDVI), the Enhanced Vegetation Index (EVI), and the Crop Water Stress Index (CWSI), with a total of 528 NDVI and EVI images and 1016 CWSI images generated through Google Earth Engine (GEE), using machine-learning techniques. Trend analyses were conducted to monitor drought patterns spatio-temporally. Our results reveal that the three-month interval is critical for effective drought monitoring and evaluation. Among the indices, SPEI emerged as the most effective for capturing drought in combination with remote-sensing data, while CWSI exhibited the highest correlation with SPEI over the three-month period, outperforming NDVI and EVI. The trend analysis indicates a significant precipitation deficit, alongside increasing trends in temperature and evapotranspiration over both the short and long term. Furthermore, all drought indices (SPI, SPEI, and RDI) demonstrate an intensification of drought conditions. Adaptation strategies are essential for managing water resources in the Upper Oum Er Rabia watershed under these evolving climate conditions. Continuous monitoring of climate variables and drought indices will be crucial for tracking changes and informing future water management strategies.

Keywords: Mediterranean; multi-index; drought monitoring; climate change; Oum Er Rabia; Morocco



Citation: Mliyah, M.M.; Ait Brahim, Y.; Koutsovili, E.-I.; Tzoraki, O.; Zian, A.; Aqnouy, M.; Benaabidate, L. Multi-Index Approach to Assess and Monitor Meteorological and Agricultural Drought in the Mediterranean Region: Case of the Upper Oum Er Rabia Watershed, Morocco. *Water* **2024**, *16*, 3104. <https://doi.org/10.3390/w16213104>

Academic Editor: Xing Yuan

Received: 6 September 2024

Revised: 12 October 2024

Accepted: 25 October 2024

Published: 29 October 2024



Copyright: © 2024 by the authors. Licensee MDPI, Basel, Switzerland. This article is an open access article distributed under the terms and conditions of the Creative Commons Attribution (CC BY) license (<https://creativecommons.org/licenses/by/4.0/>).

1. Introduction

Drought is a major natural disaster that affects regions worldwide, regardless of geographical location. While its occurrence is not confined to any specific climate zone, the impact of drought varies significantly depending on regional conditions. Some regions are less vulnerable, while others face heightened susceptibility to its effects [1]. According to the United Nations Office for Disaster Risk Reduction, more than 130 countries are affected by drought, the potential impact of which is comparable to the damage caused by the COVID-19 pandemic on people's livelihoods over the same period [2]. Due to the complexity and variability of drought, there is no universal definition of the phenomenon [3,4]. As a result, definitions are often revised [5] to better capture the diverse factors and consequences of drought on both the environment and society, as well as the intricate interactions between these two components.

Drought occurs when there is a prolonged decrease in precipitation relative to the average [6]. In some regions, high evapotranspiration demand also plays a critical role in triggering drought [7,8]. As a result of global warming, the frequency, severity, and duration of droughts are increasing, affecting more people over a longer period than any other natural disaster [9–12]. Drought is widely recognized as one of the most destructive and significant weather-related hazards [13], profoundly impacting human health, well-being, the environment, and economies [14,15]. It affects ecosystems and socioeconomic activities directly and indirectly [16–18], disrupting ecosystems and leading to severe consequences, such as river drying, oasis reduction, desertification, sandstorms, land subsidence [19], and an increase in cases of widespread forest die-off [20]. In extreme cases, drought can also increase fire risk [21,22].

The effects of drought on water resources are particularly severe, disrupting the water balance and causing a reduction in soil moisture [12,23]. It is a major contributor to soil degradation and environmental decline, as it limits vegetation growth [24]. Studies [25,26] indicate that drought accounts for about 86% of global agricultural productivity loss, significantly hindering crop growth [20] and leading to crop failure, food shortages, malnutrition, famine, mortality, and mass migration [27]. Moreover, drought can trigger political conflicts between countries over shared water resources. Its multifaceted impact spans across social security, economic stability, environmental health, and the agricultural sector [28].

In accordance with the varying effects of droughts, the authors of [29] have classified them into four categories: meteorological drought, hydrological drought, agricultural drought, and socio-economic drought. In addition to the four most common classes, [30,31] have proposed the ecological drought as a fifth class. Flash drought has been introduced as an additional category [32,33]. In addition to the aforementioned, the environmental drought is suggested. This one encompasses meteorological, hydrological, and agricultural drought [28]. The major challenge associated with drought is that all of these classes are interconnected, making it challenging to identify the commencement and termination of each class [28,34,35].

To date, drought indices have been used in numerous regions across the globe, with numerous studies having been conducted on this topic. The World Meteorological Organization (WMO) has classified these indices into five categories:

- Meteorology, e.g., Standardized Precipitation Index (SPI) [36], Drought Area Index (DAI) [37], Reconnaissance Drought Index (RDI) [38], Palmer Drought Severity Index (PDSI) [39], and Standardized Precipitation Evapotranspiration Index (SPEI) [40].
- Soil moisture, e.g., Evapotranspiration Deficit Index, Soil Moisture Deficit Index (ETDI, SMDI) [41], and Soil Water Storage (SWS) [42].
- *Hydrology*, e.g., Palmer Hydrological Drought Index (PHDI) [39], Streamflow Drought Index (SDI) [43], and Standardized Snowmelt and Rain Index (SMRI) [44].
- Remote sensing, e.g., Enhanced Vegetation Index (EVI) [45], Normalized Difference Vegetation Index (NDVI) [46,47], and Vegetation Drought Response Index (VegDRI) [48].

- Composite or modeled values, e.g., Global Integrated Drought Monitoring and Prediction System (GIDMaPS) [49], Global Land Data Assimilation System (GLDAS) [50], and U.S. Drought Monitor (USDM) [51].

A number of statistical tools are available for the purpose of checking trends and assessing changes in the various parameters used in climate change studies. The Mann–Kendall non-parametric test [52,53], proposed by the World Meteorological Organization (WMO), was used in this study to examine trends. Additionally, Sen’s Slope [54] was employed to estimate the slope of these trends.

Morocco, situated in the North African region and bordered by the Mediterranean Sea, is among the most susceptible to droughts due to its geographical location [18,55]. Over the past few years, several drought-related studies have been conducted in Morocco. A variety of techniques and indices based on ground-based and/or remotely sensed data have been used to achieve this objective [56–61]. Accordingly, the application of trend techniques has been the subject of several studies in different regions of Morocco [62–67]. The comprehensive drought analysis at both agricultural and meteorological levels is lacking, particularly with regard to the spatio-temporal trends of the drought phenomena in the Upper Oum Er Rabia watershed.

The objective of this study is to assess and monitor drought using a multi-index approach, providing an in-depth understanding of the spatio-temporal propagation of drought at both meteorological and agricultural levels within the Upper Oum Er Rabia watershed. To achieve this, we propose a methodology that combines remote-sensing temperature data (ERA5) with ground-based precipitation data to analyze the characteristics of drought using three key meteorological indices: SPI, SPEI, and RDI. Each of these indices provides unique insights into various aspects of drought conditions. The SPI focuses on precipitation deficits, and the SPEI and the RDI integrate both precipitation and evapotranspiration to assess drought severity. By leveraging these indices, the study aims to offer a comprehensive evaluation of drought patterns and intensities. Furthermore, the study incorporates three remote-sensing indices to test their capability to capture agricultural drought for 23 years, from 2000 to 2022: NDVI with 528 images, EVI with 528 images, and CWSI with 1016 images generated through Google Earth Engine, using machine-learning techniques. These indices offer valuable insights into vegetation health, productivity, and water stress under drought conditions. To monitor the spatio-temporal trends of drought, we employed trend tests such as the Mann–Kendall and Sen’s Slope tests to examine various parameters across two distinct time steps: from 1979 to 2022 and from 2010 to 2022.

2. Data and Methods

2.1. Study Area

The Oum Er Rbia (OER) watershed is one of the largest in Morocco, encompassing an area of approximately 35,000 km². It occupies 7% of the Kingdom of Morocco’s area and is responsible for a quarter of the country’s renewable water resources. This study focused on drought in the upper part of the Oum Er Rbia basin. The area of study encompasses 3,560 km², situated between latitudes 32°32′ N–33°13′ N and longitudes 5°5′ W–5°55′ W.

The Upper Oum Er Rbia (Upper OER) watershed is part of the Middle Atlas [68], and is situated in three distinct geographical areas: the Western Meseta, the Middle-Atlasic Dir and valleys, and the Middle-Atlasic cause [69]. This explains the varying altitudes, which range from 600 m in the southwest to 2400 m in the northeast. This basin encompasses four main wadis: Ouaoumana, Srou, Chbouka, and the most important, Oued Oum Er Rbia. These wadis accumulate at the Ahmed El Hansali dam. The primary source of water flow in this watershed is snowmelt, which significantly contributes to both surface and groundwater recharge [70]. In this study, the Upper Oum Er Rbia basin was divided into six sub-basins (Figure 1).

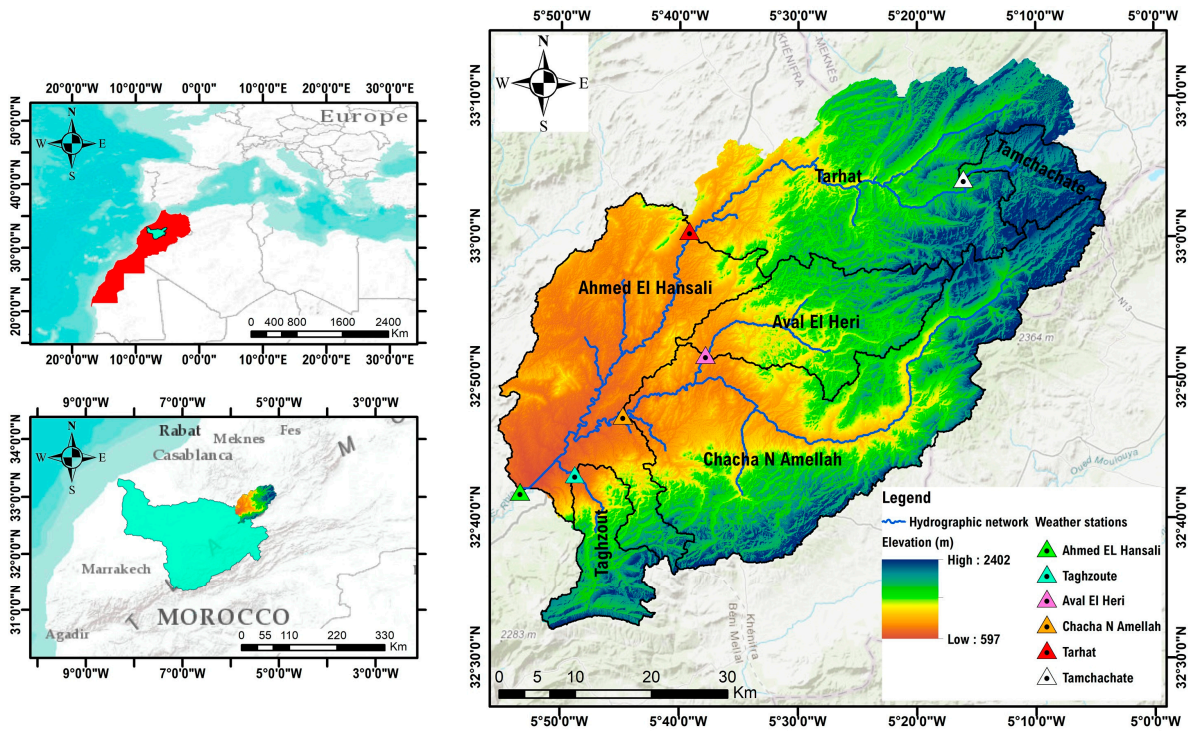


Figure 1. Location of study area.

2.2. Data Sources

2.2.1. Precipitation Data

The Upper Oum Er Rabia (Upper OER) watershed data were provided by the Oum Er Rabia Hydraulic Basin Agency (OERHBA) [71]. The dataset comprises a time series of monthly rainfall from 1979 to 2022, recorded at six rainfall stations, namely: Ahmed El Hansali (AEH), Taghzoute, Chacha N Amellah (ChachaNA), Aval El Heri (AEHeri), Tarhat and Tamchachate. The Upper OER basin receives an average annual precipitation of 559.3 mm. Among the sub-basins, the Tamchachate station records the highest rainfall at 673.9 mm/year, while the ChachaNA station records the lowest at 485.5 mm/year. The graph (Figure 2), displaying the monthly interannual rainfall variation at the sub-basin level, indicates two distinct periods: wet and dry. The wet season spans from November to April, while the remaining months are considered dry (May–October).

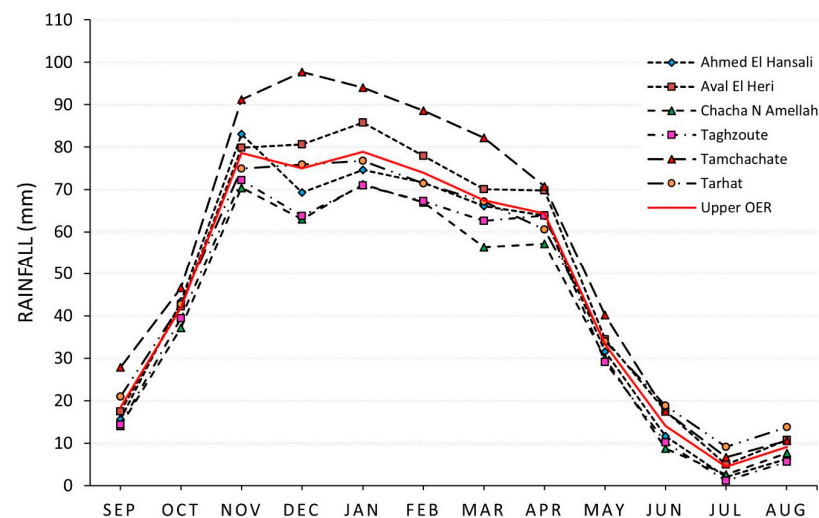


Figure 2. Average annual precipitation (1979-2022).

2.2.2. Temperature Data

In 2019, the European Centre for Medium-Range Weather Forecasts (ECMWF) unveiled the ERA5 product as part of the Copernicus Climate Change Service [72]. ERA5 represents the fifth generation of ECMWF reanalysis products [73], following ERA-Interim [74], ERA-40 [75], ERA-15 [76], and FGGE [77]. ERA5 encompasses the period from 1950 to the present day, with a spatial resolution of 31 km and a temporal resolution of up to one hour [73]. The used data were obtained from the ClimateEngine platform (<https://app.climateengine.com/climateEngine>, accessed on 13 December 2023) free of charge and with a daily time step and a spatial resolution of $0.25^\circ \times 0.25^\circ$. In order to align with the observed data, the dataset was resampled with a monthly temporal resolution from 1979 to 2022. The graph (Figure 3) displays the average monthly temperatures and potential evapotranspiration, highlighting two extreme periods: a cold period in December–January–February and a hot period in July–August–September. Tamchachate station records the lowest temperatures, while Ahmed El Hansali and Taghzoute stations record the highest.

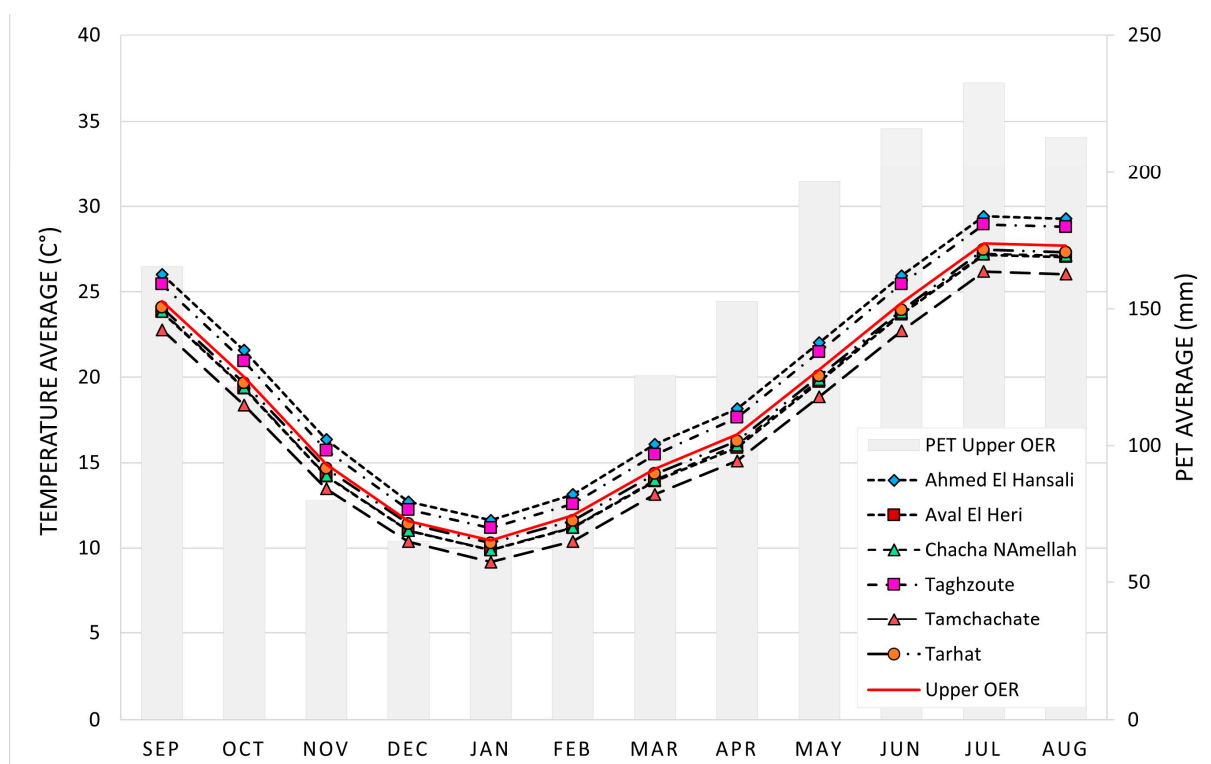


Figure 3. Average monthly temperatures and potential evapotranspiration.

2.3. Methodology

As previously stated, there are numerous drought indices, which differ according to their input data and applications. This study focuses on the analysis of drought in the Middle Atlas, with a particular emphasis on the Upper Oum Er Rbia region.

In order to achieve this objective, data from meteorological stations was used to calculate SPI, SPEI, and RDI, using RStudio 23.12. Build 402 and DrinC Version 1.7, for a period of 44 years, from 1979 to 2022. These data comprised precipitation data from meteorological stations and temperature data from ERA5 products. Remote-sensing products were used to obtain NDVI, EVI, and CWSI data using Google Earth Engine (<https://earthengine.google.com>, accessed on 28 March 2024) over the 2000–2022 period (Figure 4). Subsequently, a series of statistical tests were applied to the various datasets, including correlation tests and a trend analysis by Mann–Kendall and Sen’s Slope.

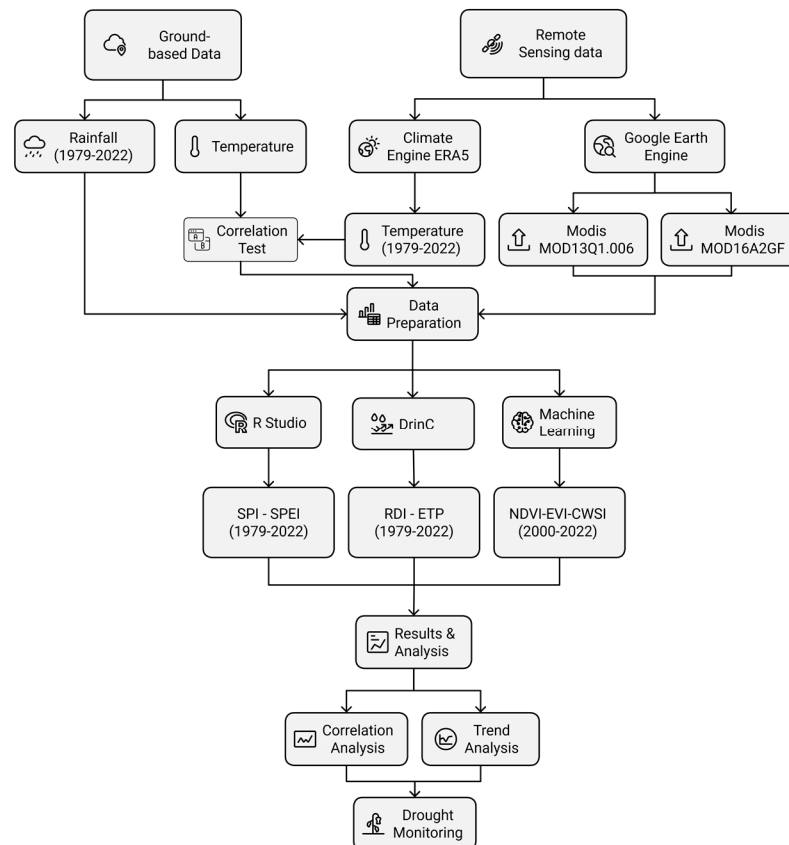


Figure 4. Flowchart of the adopted methodology.

2.3.1. Meteorological Drought Indices

The SPI [36] and the SPEI [40] are two of the most commonly utilized drought indices [78]. The SPI is an index based only on precipitation, which renders it more straightforward to employ than other indices [79]. In 2009, the World Meteorological Organization (WMO) recommended the use of the SPI to monitor the evolution of meteorological drought conditions [80]. The index's efficacy and resilience permit its application to diverse categories of drought [81]. SPEI, like SPI, is a highly versatile index that incorporates temperature data. It is an index based on precipitation and potential evapotranspiration [82]. It is sensitive to changes in evaporation requirements, similar to the PDSI [39], and can be calculated at different time scales [7]. The RDI is an index that integrates cumulative precipitation and potential evapotranspiration [83]. It has been verified and utilized successfully in numerous regions across the globe [84–87]. It is recommended that a series of consecutive years of at least 30 years be used for the calculation of the SPI, SPEI, and RDI [88,89].

- Standardized Precipitation Index (SPI)

The SPI is an index based on the probability of precipitation that employs the Gamma distribution with two statistical parameters to adjust precipitation over a specified period in relation to the average precipitation over the same period [36]. The calculation of SPI is based solely on precipitation, with other variables, such as temperature and potential evapotranspiration, being disregarded [40]. The index is calculated as follows:

$$SPI = \frac{(P - \bar{P})}{\sigma_P}$$

where (P) is the precipitation for the period, (\bar{P}) is the mean precipitation for the period, and (σ_P) is the standard deviation of precipitation for the period.

- Standardized Precipitation and Evapotranspiration Index (SPEI)

The SPEI is a probability-based index that employs the three-parameter log-logistic distribution. The calculation of SPEI is analogous to that of the SPI, with a single notable distinction; indeed, it incorporates potential evapotranspiration, as evidenced by the demonstrated influence of precipitation and temperature on drought response [8,90]. The SPEI employs the difference between precipitation and ETP to calculate the index, and it was developed based on the water-balance concept of climatic water supply and atmospheric evaporative demand [40]. The index is calculated as follows:

$$SPEI = \frac{(P - PET - \bar{D})}{\sigma_D}$$

where (P) is the precipitation, (PET) is the potential evapotranspiration, (\bar{D}) is the mean of the difference (P—PET), and σ_D is the standard deviation of the difference (P—PET).

- Reconnaissance Drought Index (RDI)

The RDI [38] is similarly based on the ratio of precipitation and potential evapotranspiration factors [91]. The calculation of this index integrates the principal inputs and outputs of a natural water system, rendering it highly pertinent for the estimation of water availability [87]. The index is calculated as follows:

$$RDI = \frac{(P/PET - \bar{R})}{\sigma_R}$$

where (P) is the precipitation, (PET) is the potential evapotranspiration, (\bar{R}) is the mean of the ratio (P/PET), and (σ_R) is the standard deviation of the ratio (P/PET).

2.3.2. Classification Criteria

In the current study, drought is defined as occurring when the value of the intensity of SPI, SPEI, and RDI indices is equal to (−1) and ending when the intensity of those indices reaches zero. SPI values are classified according to their intensities (Table 1) in a similar way to SPEI and RDI.

Table 1. Classification of drought intensity according to [37].

SPI/SPEI/RDI	Category
−0.99 to 0.99	Near normal
−1.0 to −1.49	Moderately dry
−1.5 to −1.99	Severely dry
−2 and less	Extremely dry

2.3.3. Agricultural Remote Sensing Drought Indices

Agricultural drought reflects soil moisture status and crop health, indicating soil water deficit relative to crop needs [92]. The use of remote-sensing techniques enables effective monitoring and diagnosis of vegetation water status, accurately reflecting the physiological condition of vegetation under water stress, and facilitates rapid drought detection and the immediate implementation of irrigation measures [93–96].

The Normalized Difference Vegetation Index (NDVI) and Enhanced Vegetation Index (EVI), as well as the Crop Water Stress Index (CWSI), are indices that enable spatio-temporal assessment and monitoring of vegetation via remote sensing. They have been widely used to monitor the occurrence of agricultural drought, for example, in [97–102].

In this study, the aforementioned indices were established using machine-learning techniques. The first two indices utilized were derived from the MODIS MOD13Q1.006 Terra Vegetation Indices product (<https://doi.org/10.5067/MODIS/MOD13Q1.006>, accessed on

7 October 2023), while the third index was derived from the MODIS MOD16A2GF Version 6.1 (<https://doi.org/10.5067/MODIS/MOD16A2GF.061>, accessed on 28 March 2024).

These indices have been pre-corrected, thereby eliminating undesirable effects such as water, clouds, heavy aerosols, and cloud shadows. A total of 528 images were analyzed for each index (NDVI and EVI), and 1016 images were analyzed for (CWSI), using the Google Earth Engine platform. The dataset encompasses the period from 2000 to 2022, with 250 m resolution images captured every 16 days for NDVI and EVI, and 500 m resolution images captured every 8 days for CWSI.

- Normalized Difference Vegetation Index and Enhanced Vegetation Index

The Normalized Difference Vegetation Index (NDVI) quantifies the density and green color of vegetation, while the Enhanced Vegetation Index (EVI) attenuates variations in the canopy background while maintaining sensitivity to areas of dense vegetation.

- Crop Water Stress Index

The Crop Water Stress Index (CWSI) [103,104] is a widely accepted metric for assessing plant hydration across various spatial scales. This index, based on the principles of energy balance, enables the real-time monitoring of drought conditions by taking into account soil moisture and farmland evapotranspiration [99]. Idso et al. [103] initially proposed the CWSI by establishing an empirical correlation between canopy temperature and the air vapor pressure deficit. Subsequently, Jackson [104] provided a theoretical interpretation based on the energy balance of the canopy, leading to a refined calculation of the CWSI ($CWSI = 1 - ET/PET$), where ET represents evapotranspiration and PET represents potential evapotranspiration. The index ranges from zero (0) to one (1), with lower values indicating wetter conditions and higher values indicating drier conditions. For the current study, we specifically used 1-CWSI, so that lower values indicate drier conditions and higher values indicate wetter conditions, aligning with other indices. This definition has since been used in numerous studies [105–108].

2.3.4. Google Earth Engine (GEE)

Google Earth Engine is a cloud-based platform for geospatial analysis, which is powered by Google's supercomputers. It integrates multi-petabyte remote-sensing products from over 40 years of data, including Sentinel 1, 2, 3, and 5P; Landsat 1–5, 4, 5, 7, 8, and 9; Advanced Land Observing Satellite (ALOS) products; MODIS products; and others [109]. The GEE offers a large number of ready-to-use products, including Normalized Difference Vegetation Index (NDVI) and Enhanced Vegetation Index (EVI), which can be accessed via an application programming interface (API). This API is executable via JavaScript from Code Editor (<https://earthengine.google.com>, accessed on 28 March 2024). This study required the use of machine learning since it may greatly improve remote-sensing research by automating processes, increasing accuracy, and extracting valuable insights from vast amounts of data.

2.3.5. Trend Tests

- Mann–Kendall test

The non-parametric Mann–Kendall statistical test [52,53] is one of the most widely used tests in environmental studies for assessing the trend of desired data time series. This test compares, sequentially, each data item in a time series with the remaining data.

- Sen's Slope method

The Sen's Slope method [54] is used in conjunction with the Mann–Kendall test, which determines the magnitude of the trend resulting from the Mann–Kendall test and expresses it as a slope (the change in the data examined per unit of time).

For this study, Mann–Kendall and Sen's Slope are applied to precipitation, temperature, evapotranspiration, SPI, SPEI, and RDI to examine trends, upward or downward, at the level of the study area.

3. Results and Discussion

This investigation used ERA5 temperature data due to the limited availability of weather stations in the study area. Indeed, only two weather stations exist: (1) Ahmed El Hansali and (2) Tarhat, provided by (OERHBA) during (1985–1998 and 2009–2021) and (1985–2021), respectively, in a monthly time step. In light of the limited number of meteorological stations, we used correlation tests between both stations data (monthly, minimum, and maximum temperatures) and the reanalysis products. The results of these tests indicated a strong correlation between the variables (Figure 5), which reinforced the decision to utilize ERA5 data for the analysis. This choice allowed us to overcome the limitations posed by the sparse station coverage and leverage the comprehensive global estimates provided by ERA5.

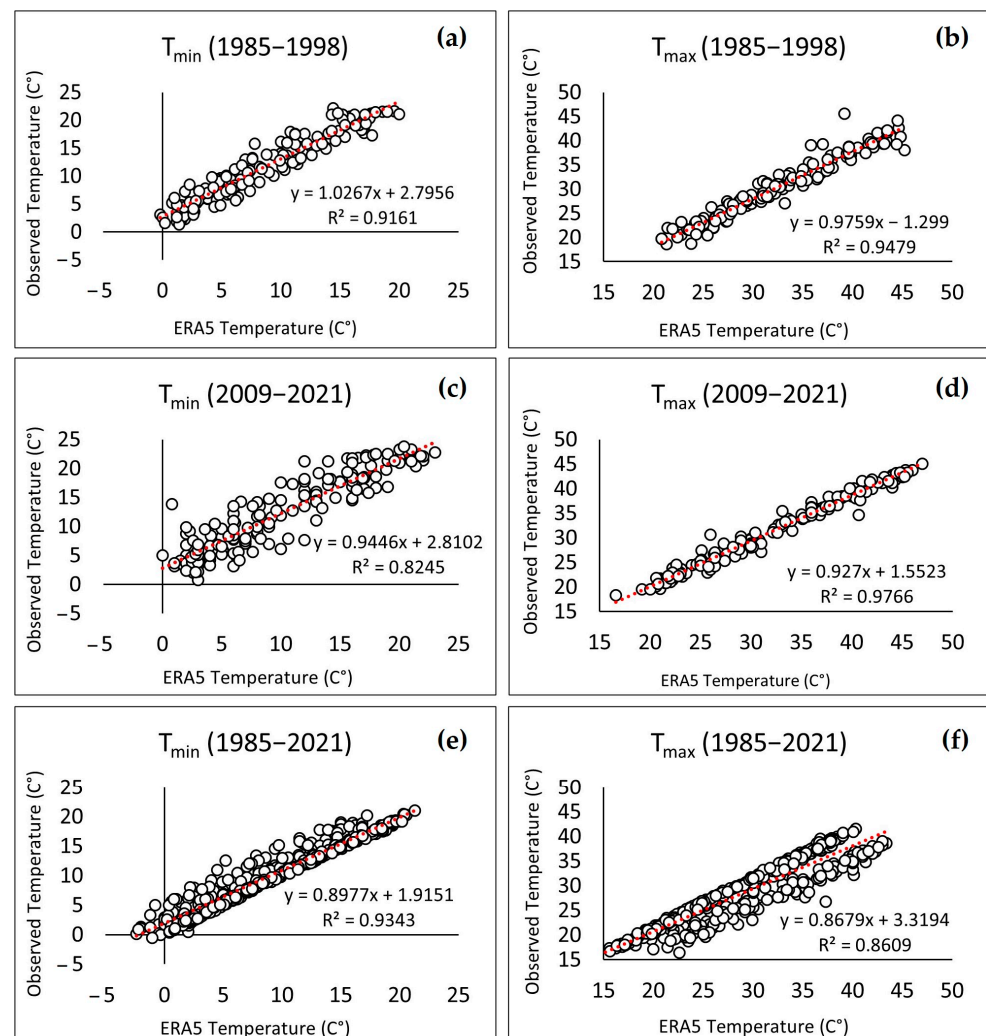


Figure 5. Correlation graphs between observed temperatures and ERA5 product temperatures: (a–d) Ahmed El Hansali station and (e,f) Tarhat station.

3.1. Drought Characteristics Analysis

3.1.1. Drought Duration

The study of drought in the Upper Oum Er Rbia basin was conducted over a 44-year period (1979–2022). Table 2 presents the duration, in months, of each event of the three drought indices (SPI, SPEI, and RDI) for each sub-basin, according to the time step (1, 3, 6, and 12 months). Tamchachate, with a total of 96 months (19% of the total duration) for the 1-month time step, is the sub-basin most affected by drought, followed by AEHeri (82 months, 16%), Taghzoute (81 months, 16%), and then the other sub-basins. For the three-

month time step, Taghzoute and Tamchachate exhibited the longest duration of drought months, with (145 months, 28%) and (143 months, 28%), respectively. This was followed by Tarhat with (136 months, 26%) and then the other sub-basins. The longest duration for the six-month time step is that of the AEHeri sub-basin, with (159 months, 31%), followed by the other sub-basins with very similar durations, except for Ahmed El Hansali. The drought durations in the AEH, AEHeri, and Taghzoute sub-basins are (160 months, 32%), (155 months, 31%), and (153 months, 30%), respectively. For monthly time steps of one, three, six, and twelve months, the average number of dry months for all sub-basins is 78, 129, 146, and 141 months, respectively. For the Upper Oum Er Rbia watershed as a whole, the number of dry months is nearly identical to the average for all sub-basins.

Table 2. Duration of drought at sub-basin level and Upper OER basin.

Time Step	Ahmed El Hansali	Taghzoute	Chacha N Amellah	Aval El Heri	Tarhat	Tamchachate	Upper OER
1 month	75	81	59	82	72	96	76
3 months	109	145	116	123	136	143	132
6 months	131	147	144	159	149	147	151
12 months	160	153	122	155	125	128	147

3.1.2. Drought Intensity

In accordance with the categorization of drought severity into three classes (moderate, severe, and extreme) and with a focus on the sub-basin level analysis, drought indices have been computed at four time steps (1, 3, 6, and 12 months) and are presented in detail in (Table 3). For all sub-basins, the highest number of months with moderate drought was observed when the time step was set to 12 months. The majority of sub-basins exhibited the highest number of months with severe drought when calculated using a 12-month time step, with the exception of the Taghzoute sub-basin, where the 6-month time step yielded the most months with severe drought. With regard to extreme drought, the results indicate that the 3-month time step yielded the greatest number of dry months, with the exception of the Ahmed El Hansali sub-basin, where the 6-month time step produced the greatest number of months with extreme drought.

Table 3. Percentage of months with drought intensity per time step.

Ahmed El Hansali	SPI1	SPEI1	RDI1	SPI3	SPEI3	RDI3	SPI6	SPEI6	RDI6	SPI 12	SPEI 12	RDI 12
Normal Drought	9.3	6.2	8.5	9.9	8.4	9.7	10.6	11.0	11.0	48.8	53.8	48.8
Moderate Drought	2.3	6.2	3.5	5.4	6.8	4.9	9.0	8.8	8.6	30.6	26.9	27.5
Severe Drought	1.6	1.7	2.1	2.7	4.9	4.7	3.1	4.5	3.1	16.3	15.6	18.8
Extreme Drought	1.4	0.4	0.2	3.1	1.2	1.4	2.5	1.4	2.7	4.4	3.8	5.0
Taghzoute	SPI1	SPEI1	RDI1	SPI3	SPEI3	RDI3	SPI6	SPEI6	RDI6	SPI 12	SPEI 12	RDI 12
Normal Drought	10.7	8.1	10.1	13.8	13.4	13.6	11.4	11.7	10.4	12.3	12.3	10.3
Moderate Drought	2.5	5.8	4.7	8.2	8.6	9.1	10.8	12.1	12.1	13.5	12.3	14.3
Severe Drought	1.6	1.6	1.0	3.7	5.3	3.9	4.5	4.3	4.3	3.4	4.8	4.4
Extreme Drought	1.0	0.2	0.0	2.5	1.0	1.6	2.2	0.6	2.0	1.2	1.0	1.4
Chacha N Amellah	SPI1	SPEI1	RDI1	SPI3	SPEI3	RDI3	SPI6	SPEI6	RDI6	SPI 12	SPEI 12	RDI 12
Normal Drought	6.4	4.8	7.2	10.7	8.4	12.5	12.9	10.8	17.6	5.1	5.7	13.7
Moderate Drought	2.5	5.0	2.7	6.6	9.7	5.4	10.4	11.7	5.1	13.3	11.1	4.8
Severe Drought	1.2	0.8	1.6	3.1	3.5	3.1	3.9	4.7	3.7	5.1	7.3	4.4
Extreme Drought	1.4	0.8	0.0	2.1	1.0	1.6	1.0	1.0	1.8	0.6	0.0	1.4
Aval El Heri	SPI1	SPEI1	RDI1	SPI3	SPEI3	RDI3	SPI6	SPEI6	RDI6	SPI 12	SPEI 12	RDI 12
Normal Drought	9.9	8.5	11.2	10.7	10.1	10.9	16.4	15.3	15.7	16.0	12.1	14.1
Moderate Drought	3.3	5.0	2.7	8.0	8.8	8.6	10.0	9.8	10.2	8.9	12.3	10.3
Severe Drought	1.6	1.6	1.9	3.1	4.1	2.3	3.1	5.1	3.5	5.5	5.1	6.1
Extreme Drought	1.2	0.8	0.0	2.1	1.0	2.1	1.6	1.0	1.8	0.2	1.2	0.2

Table 3. Cont.

Tarhat	SPI1	SPEI1	RDI1	SPI3	SPEI3	RDI3	SPI6	SPEI6	RDI6	SPI 12	SPEI 12	RDI 12
Normal Drought	8.3	8.1	10.3	14.2	10.5	16.0	14.5	11.7	18.2	5.9	5.9	12.9
Moderate Drought	3.1	4.1	2.9	6.8	11.5	5.4	10.0	11.7	5.5	13.1	11.5	6.9
Severe Drought	1.9	1.2	0.8	3.3	3.5	2.3	3.7	4.7	4.3	5.1	7.3	4.6
Extreme Drought	0.6	0.6	0.0	2.1	1.0	2.7	1.0	1.0	1.2	0.6	0.0	0.4
Tamchachate	SPI1	SPEI1	RDI1	SPI3	SPEI3	RDI3	SPI6	SPEI6	RDI6	SPI 12	SPEI 12	RDI 12
Normal Drought	12.6	8.9	13.2	14.4	11.9	13.8	13.3	11.5	11.7	5.9	6.3	5.5
Moderate Drought	2.5	6.6	4.7	7.8	11.5	8.8	10.6	11.5	12.3	13.7	11.7	11.5
Severe Drought	2.7	2.3	0.8	3.5	3.5	4.1	3.9	4.7	3.5	5.1	7.3	7.3
Extreme Drought	0.8	0.8	0.0	2.1	1.0	1.2	1.0	1.0	1.2	0.6	0.0	1.0

3.2. Multivariate Analysis of Precipitation, Drought Indices, and Remote-Sensing Indices

In this study, we used a dataset comprising precipitation and temperature records spanning the period from 1979 to 2022. These data were used as the basis for calculating three key drought indices: the Standardized Precipitation Index (SPI), the Standardized Precipitation Evapotranspiration Index (SPEI), and the Reconnaissance Drought Index (RDI). Furthermore, we incorporated remote-sensing data spanning the period from 2000 to 2022. In order to align with the available data, we established correlations at two temporal scales.

3.2.1. Correlation Analysis at Sub-Basins Level

A correlation analysis of the data in (Table 4) revealed a strong correlation between the drought indices SPI, SPEI, and RDI for the different time steps of 1, 3, 6, and 12 months and annual, with a *p*-value less than 0.001. However, this correlation was not significant for the Tarhat sub-basin, where RDI/SPI and RDI/SPEI exhibited a non-significant correlation. The majority of sub-basins exhibited a moderate correlation between precipitation and drought indices at the 1-month time step. However, at the Tarhat sub-basin level, the correlation was non-significant. The strongest correlation between precipitation and drought indices was observed at the annual time step.

However, our analysis of NDVI and drought indices at the annual time step revealed no correlation, with the exception of the AEHansali sub-basin. In contrast, the remaining sub-basins exhibited a positive correlation, although relatively weak. Nonetheless, the analysis indicated that there was no correlation between drought indices and NDVI at any given time step within the Tamchachate sub-basin. The AEHansali sub-basin exhibited the most significant correlation results for both the annual and 6-month time steps. The correlation coefficients for NDVI/SPI and NDVI/SPEI were 0.610 and 0.437, respectively, with *p*-values of less than 0.01 and less than 0.001. The correlation between EVI, drought indices, and precipitation is lower than that between NDVI and the latter. The best correlations are obtained for the annual and 6-month time steps in the AEH sub-basin. The same applies to the EVI/precipitation relationship, where the only correlation, but weak, was obtained in the same sub-basin. The correlation between CWSI, drought indices, and precipitation is notably stronger than that between NDVI and EVI and drought indices. The correlation results with a three-month time step are the most relevant for CWSI (Figure 6). In addition, the correlation between CWSI/SPEI shows better results than that between CWSI/SPI and RDI. The correlation coefficients for these results range from 0.472 to 0.504 with a *p*-value of less than 0.001. Furthermore, the correlation with the annual time step, as well as that between CWSI/precipitation, still shows good results, with coefficients ranging from 0.661 to 0.806 and from 0.706 to 0.755, respectively, with a *p*-value of less than 0.001.

Table 4. Correlation between precipitation, SPI, SPEI, RDI, NDVI, EVI, and CWSI with different time steps: (a) Ahmed El Hansali, (b) Taghzoute, (c) Chacha N Amellah, (d) Aval El Heri, (e) Tarhat, and (f) Tamchachate (***p*-value < 0.01, ***p*-value < 0.01, and **p*-value < 0.05).

Correlation	(a)	1	3	6	12	Annual	(b)	1	3	6	12	Annual
SPEI/SPI	1979–2022	0.767 ***	0.858 ***	0.906 ***	0.942 ***	0.931 ***	1979–2022	0.782 ***	0.868 ***	0.934 ***	0.945 ***	0.940 ***
RDI/SPI		0.871 ***	0.962 ***	0.990 ***	0.995 ***	0.995 ***		0.845 ***	0.956 ***	0.991 ***	0.995 ***	0.996 ***
RDI/SPEI		0.870 ***	0.902 ***	0.938 ***	0.966 ***	0.960 ***		0.858 ***	0.907 ***	0.958 ***	0.969 ***	0.967 ***
PRCP/SPI		0.680 ***	0.460 ***	0.363 ***	0.271 ***	0.990 ***		0.682 ***	0.458 ***	0.364 ***	0.237 ***	0.992 ***
PRCP/SPEI		0.685 ***	0.457 ***	0.352 ***	0.239 ***	0.915 ***		0.681 ***	0.450 ***	0.341 ***	0.202 ***	0.925 ***
PRCP/RDI		0.685 ***	0.470 ***	0.361 ***	0.262 ***	0.984 ***		0.637 ***	0.462 ***	0.362 ***	0.228 ***	0.987 ***
NDVI/SPI	2000–2022	0.04	0.255 ***	0.351 ***	0.289 ***	0.610 **	2000–2022	0.013	0.111	0.198 **	0.263 ***	0.265
NDVI/SPEI		0.194 **	0.358 ***	0.437 ***	0.294 ***	0.573 **		0.062	0.153 *	0.226 ***	0.260 ***	0.193
NDVI/RDI		0.085	0.280 ***	0.364 ***	0.287 ***	0.600 **		−0.098	0.085	0.193 **	0.267 ***	0.242
NDVI/PRCP		0.392 ***				0.586 **		0.321 ***				0.27
EVI/SPI		0.016	0.187 **	0.305 ***	0.262 ***	0.634 **		0.049	0.088	0.134 *	0.249 ***	0.367
EVI/SPEI		0.12	0.271 ***	0.389 ***	0.261 ***	0.609 **		−0.017	0.056	0.152 *	0.254 ***	0.317
EVI/RDI		0.064	0.208 ***	0.317 ***	0.261 ***	0.627 **		−0.025	0.048	0.12	0.254 ***	0.346
EVI/PRCP		0.222 ***				0.602 **		−0.008				0.365
EVI/NDVI		0.911 ***				0.987 ***		0.680 ***				0.884 ***
CWSI/SPI		0.301 ***	0.384 ***	0.356 ***	0.193 **	0.702 ***		0.356 ***	0.383 ***	0.383 ***	0.217 ***	0.692 ***
CWSI/SPEI		0.482 ***	0.504 ***	0.427 ***	0.191 **	0.719 ***		0.464 ***	0.477 ***	0.428 ***	0.199 **	0.721 ***
CWSI/RDI		0.336 ***	0.416 ***	0.369 ***	0.187 **	0.718 ***		0.265 ***	0.396 ***	0.394 ***	0.215 ***	0.708 ***
CWSI/PRCP		0.737 ***				0.697 ***		0.755 ***				0.715 ***
CWSI/NDVI		0.732 ***				0.562 **		0.491 ***				0.208
CWSI/EVI	0.538 ***				0.584 **	0.055				0.32		
Correlation	(c)	1	3	6	12	Annual	(d)	1	3	6	12	Annual
SPEI/SPI	1979–2022	0.781 ***	0.912 ***	0.964 ***	0.976 ***	0.976 ***	1979–2022	0.812 ***	0.913 ***	0.953 ***	0.960 ***	0.960 ***
RDI/SPI		0.889 ***	0.664 ***	0.722 ***	0.764 ***	0.767 ***		0.872 ***	0.978 ***	0.997 ***	0.996 ***	0.996 ***
RDI/SPEI		0.871 ***	0.678 ***	0.706 ***	0.736 ***	0.739 ***		0.909 ***	0.930 ***	0.968 ***	0.979 ***	0.979 ***
PRCP/SPI		0.675 ***	0.359 ***	0.304 ***	0.194 ***	0.749 ***		0.686 ***	0.483 ***	0.404 ***	0.297 ***	0.982 ***
PRCP/SPEI		0.680 ***	0.354 ***	0.281 ***	0.173 ***	0.700 ***		0.695 ***	0.473 ***	0.375 ***	0.269 ***	0.926 ***
PRCP/RDI		0.694 ***	0.454 ***	0.357 ***	0.247 ***	0.987 ***		0.708 ***	0.486 ***	0.399 ***	0.291 ***	0.976 ***

Table 4. Cont.

Correlation	(c)	1	3	6	12	Annual	(d)	1	3	6	12	Annual
NDVI/SPI	2000–2022	0.01	0.186 **	0.246 ***	0.217 ***	0.299	2000–2022	0.006	0.172 **	0.249 ***	0.246 ***	0.247
NDVI/SPEI		0.087	0.236 ***	0.265 ***	0.214 ***	0.24		0.12	0.202 ***	0.261 ***	0.220 ***	0.14
NDVI/RDI		−0.019	0.096	0.193 **	0.260 ***	0.24		0.021	0.151 *	0.243 ***	0.246 ***	0.217
NDVI/PRCP		0.289 ***				0.254		0.340 ***				0.218
EVI/SPI		0.002	0.118	0.225 ***	0.213 ***	0.349		−0.009	0.1	0.177 **	0.226 ***	0.265
EVI/SPEI		−0.006	0.147 *	0.254 ***	0.218 ***	0.314		0	0.097	0.207 ***	0.220 ***	0.203
EVI/RDI		−0.035	0.065	0.146 *	0.256 ***	0.342		−0.011	0.087	0.173 **	0.235 ***	0.247
EVI/PRCP		0.018				0.333		−0.013				0.235
EVI/NDVI		0.815 ***						0.640 ***				0.858 ***
CWSI/SPI		0.307 ***	0.417 ***	0.388 ***	0.116	0.704 ***		0.303 ***	0.402 ***	0.410 ***	0.240 ***	0.733 ***
CWSI/SPEI		0.467 ***	0.489 ***	0.400 ***	0.106	0.726 ***		0.454 ***	0.491 ***	0.440 ***	0.228 ***	0.743***
CWSI/RDI		0.325 ***	0.359 ***	0.354 ***	0.071	0.661 ***		0.322 ***	0.411 ***	0.414 ***	0.237 ***	0.743***
CWSI/PRCP		0.740 ***				0.671 ***		0.706 ***				0.745***
CWSI/NDVI		0.536 ***				0.286		0.670 ***				0.331
CWSI/EVI	0.182 **				0.364	0.246 ***				0.411		
Correlation	(e)	1	3	6	12	Annual	(f)	1	3	6	12	Annual
SPEI/SPI	1979–2022	0.772 ***	0.912 ***	0.964 ***	0.976 ***	0.976 ***	1979–2022	0.771 ***	0.912 ***	0.964 ***	0.976 ***	0.976 ***
RDI/SPI		0.032	0.696 ***	0.772 ***	0.822 ***	0.836 ***		0.844 ***	0.958 ***	0.996 ***	0.995 ***	0.996 ***
RDI/SPEI		0.022	0.733 ***	0.781 ***	0.829 ***	0.840 ***		0.914 ***	0.960 ***	0.979 ***	0.990 ***	0.991 ***
PRCP/SPI		0.014	0.469 ***	0.389 ***	0.265 ***	0.989 ***		0.522 ***	0.363 ***	0.297 ***	0.184 ***	0.743 ***
PRCP/SPEI		0.03	0.467 ***	0.372 ***	0.244 ***	0.954 ***		0.541 ***	0.360 ***	0.278 ***	0.168 ***	0.708 ***
PRCP/RDI		0.571 ***	0.364 ***	0.304 ***	0.205 ***	0.826 ***		0.526 ***	0.371 ***	0.296 ***	0.179 ***	0.735 ***
NDVI/SPI	2000–2022	0.09	0.173 **	0.214 ***	0.201 **	0.299	2000–2022	−0.026	−0.012	−0.005	0.059	0.023
NDVI/SPEI		0.155 *	0.220 ***	0.223 ***	0.205 ***	0.245		−0.035	−0.015	−0.019	0.072	−0.015
NDVI/RDI		−0.008	0.094	0.211 ***	0.269 ***	0.271		−0.096	−0.032	−0.024	0.064	0.002
NDVI/PRCP		0.311 ***				0.337		0.004				0.001
EVI/SPI		0.079	0.109	0.202 ***	0.197 **	0.347		−0.048	0	0.049	0.101	0.174
EVI/SPEI		0.144 *	0.134 *	0.225 ***	0.209 ***	0.323		−0.075	−0.007	0.047	0.117	0.149
EVI/RDI		−0.032	0.07	0.164 **	0.267 ***	0.373		−0.1	−0.022	0.028	0.106	0.157
EVI/PRCP		0.012				0.333		−0.101				0.158
EVI/NDVI		0.783 ***				0.928 ***		0.917 ***				0.936 ***

Table 4. Cont.

Correlation	(e)	1	3	6	12	Annual	(f)	1	3	6	12	Annual
CWSI/SPI	2000–2022	0.176 **	0.418 ***	0.392 ***	0.219 ***	0.718 ***	2000–2022	0.360 ***	0.402 ***	0.357 ***	0.184 **	0.666 ***
CWSI/SPEI		0.242 ***	0.493 ***	0.406 ***	0.213 ***	0.743 ***		0.472 ***	0.472 ***	0.365 ***	0.176 **	0.696 ***
CWSI/RDI		0.328 ***	0.371 ***	0.392 ***	0.229 ***	0.806 ***		0.360 ***	0.432 ***	0.364 ***	0.184 **	0.681 ***
CWSI/PRCP				0.726 ***		0.707 ***				0.728 ***		0.696 ***
CWSI/NDVI				0.510 ***		0.271				−0.109		−0.084
CWSI/EVI				0.163 **		0.354				−0.245 ***		0.066

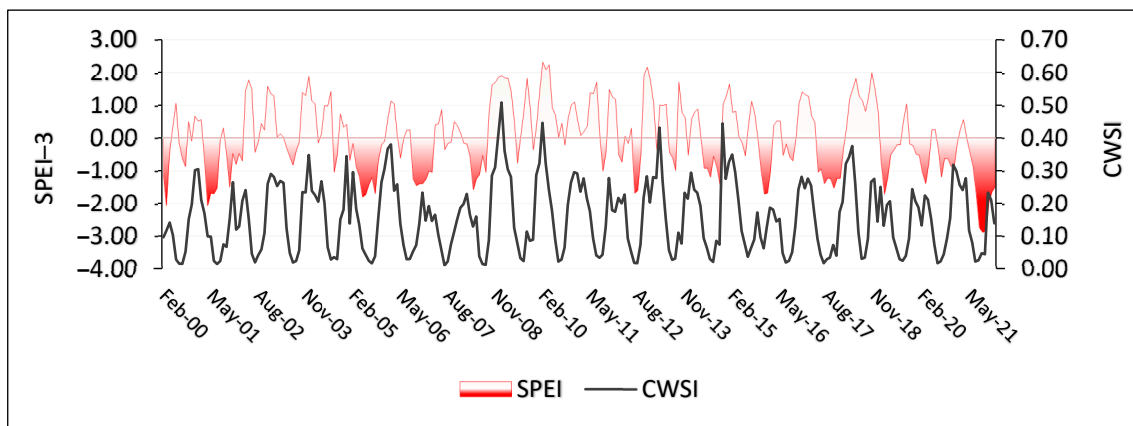


Figure 6. Graph of monthly SPEI (3 months) and CWSI.

Taking a close look at the best correlation results obtained among SPEI/NDVI, SPEI/EVI, and SPEI/CWSI, it is observed that the correlation between these variables across different seasons is interesting (Table 5). For the SPEI6/NDVI correlation, the results during summer, fall, and winter are 0.582, 0.577, and 0.572, respectively. These values suggest a moderate correlation, substantiated by a *p*-value less than 0.05. Conversely, the spring season exhibits a strong correlation of 0.739, supported by a *p*-value less than 0.001. In a similar vein, the spring season also demonstrates a strong correlation of 0.746 for SPEI6/EVI, with a *p*-value less than 0.001. The other seasons, however, display a moderate correlation that fluctuates with the change in seasons: 0.556 for summer (*p*-value < 0.05), and 0.447 and 0.502 for fall and winter, respectively (*p*-value < 0.1). Parallel results were discerned for the correlation between SPEI3/CWSI. Here, the spring season outperformed the other seasons, exhibiting a very strong correlation of 0.821 (*p*-value < 0.001) (Figure 7). The remaining seasons also demonstrated a strong correlation: 0.610 and 0.632 for summer and fall, respectively (*p*-value < 0.05). Winter, too, displayed a strong correlation, supported by a *p*-value less than 0.001.

Table 5. Correlation between SPEI6/NDVI, SPEI6/EVI, and SPEI3/CWSI in different seasons (***p*-value < 0.01, *** *p*-value < 0.001, and * *p*-value < 0.05).

Correlation	Fall	Spring	Summer	Autumn
SPEI6/NDVI	0.572 **	0.739 ***	0.582 **	0.577 **
SPEI6/EVI	0.502 *	0.746 ***	0.556 **	0.447 *
SPEI3/CWSI	0.668 ***	0.821 ***	0.610 **	0.632 **

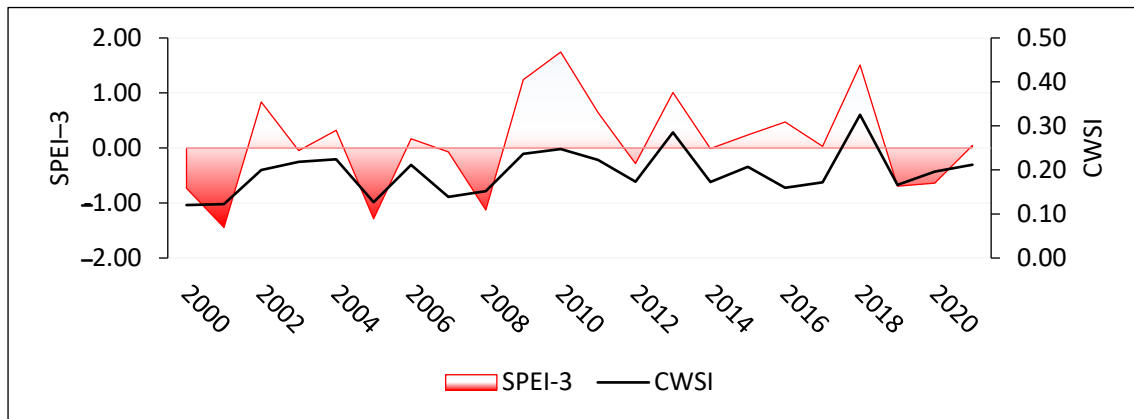


Figure 7. Graph of SPEI (3 months) and CWSI in the spring season.

3.2.2. Correlation Analysis at Watershed Level

A correlation analysis of drought indices (SPI, SPEI, and RDI) at the Upper OER basin level (Figure 8) revealed a consistently strong relationship at each time step (Table 6). The correlation coefficient reached 0.996 with a *p*-value less than 0.001 between RDI and SPI at the 3- and 6-month time steps. The relationship between drought indices and precipitation is characterized by a strong and moderate correlation with a *p*-value less than 0.001 at annual and 1-month time steps, respectively. For other time steps, the correlation is weak. The 12-month time step shows no correlation.

However, the relationship between remote-sensing indices (NDVI, EVI, and CWSI) and drought indices showed a non-significant-to-weak correlation. The best value was found between NDVI/SPEI and EVI/SPEI (at a 6-month time step) and between CWSI/SPEI (at a 3-month time step), with values of 0.336, 0.302, and 0.335, respectively, with *p*-value less than 0.001. Moreover, with an annual time step, the best correlation values were observed between CWSI and SPI/SPEI/RDI (over 0.75 with a *p*-value less than 0.001).

Table 6. Correlation between precipitation, SPI, SPEI, RDI, NDVI, and EVI with different time steps at Upper OER basin level (***p*-value < 0.001, **p*-value < 0.01, and **p*-value < 0.05).

	Correlation	1 Month	3 Months	6 Months	12 Months	Annual
1979–2022	SPEI/SPI	0.828 ***	0.900 ***	0.943 ***	0.949 ***	0.947 ***
	RDI/SPI	0.940 ***	0.996 ***	0.996 ***	0.994 ***	0.995 ***
	RDI/SPEI	0.875 ***	0.920 ***	0.964 ***	0.974 ***	0.974 ***
	PRCP/SPI	0.657 ***	0.456 ***	0.377 ***	0.054	0.992 ***
	PRCP/SPEI	0.681 ***	0.449 ***	0.350 ***	0.062	0.930 ***
	PRCP/RDI	0.681 ***	0.459 ***	0.371 ***	0.056	0.985 ***
2000–2022	NDVI/SPI	0.055	0.202 ***	0.294 ***	0.295 ***	0.421 *
	NDVI/SPEI	0.137 *	0.270 ***	0.336 ***	0.279 ***	0.339
	NDVI/RDI	0.067	0.198 **	0.290 ***	0.298 ***	0.395
	NDVI/PRCP			0.367 ***		0.481 *
	EVI/SPI	0.011	0.150 *	0.253 ***	0.293 ***	0.419 *
	EVI/SPEI	0.038	0.188 **	0.302 ***	0.283 ***	0.462 *
	EVI/RDI	−0.001	0.144 *	0.249 ***	0.297 ***	0.454 *
	EVI/PRCP			0.095		0.602 **
	EVI/NDVI	0.829 ***	0.829 ***	0.829 ***	0.829 ***	0.930 ***
	CWSI/SPI	0.201 **	0.255 ***	0.251 ***	0.117	0.763 ***
	CWSI/SPEI	0.328 ***	0.335 ***	0.276 ***	0.103	0.764 ***
	CWSI/RDI	0.233 ***	0.278 ***	0.260 ***	0.111	0.773 ***
	CWSI/PRCP			0.593 ***		0.768 ***
	CWSI/NDVI			0.366 ***		0.365
CWSI/EVI			−0.029		0.428 *	

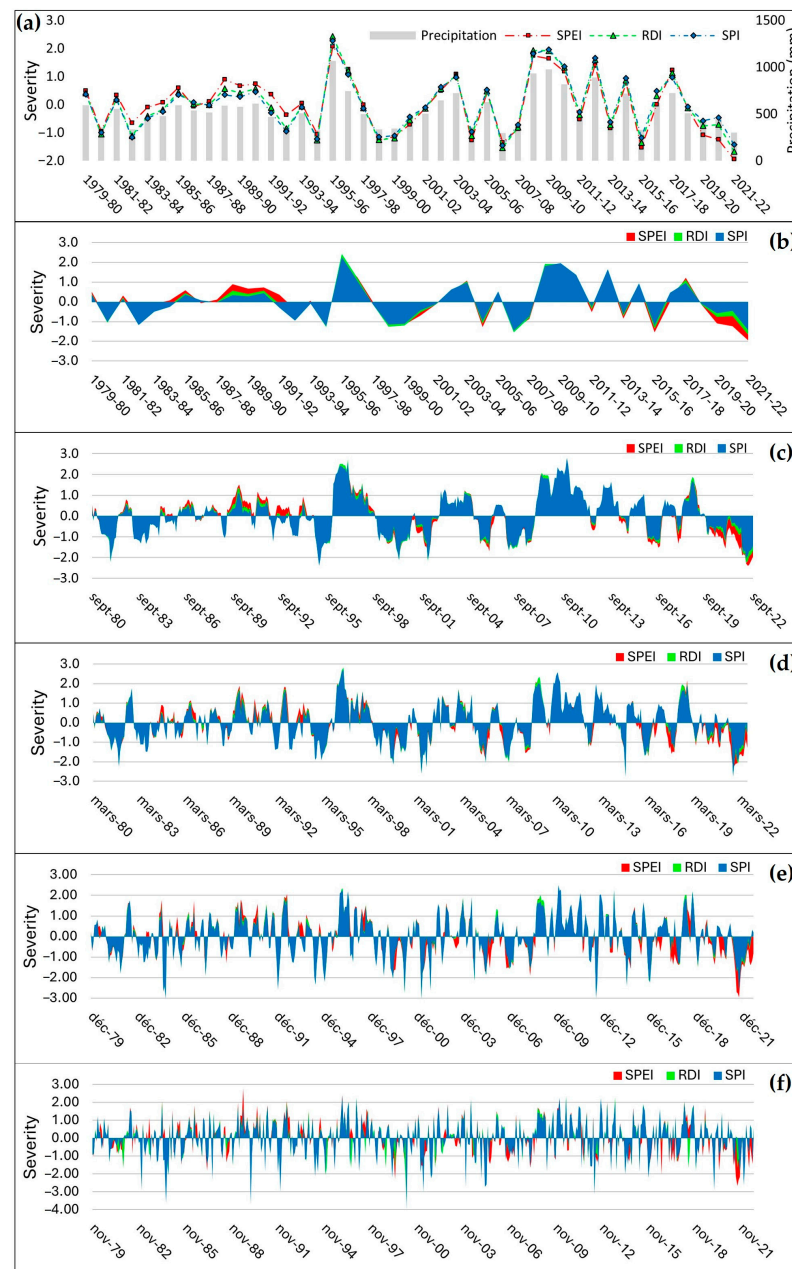


Figure 8. (a) Annual precipitation, SPEI, RDI and SPI, (b) annual, (c) 12 months, (d) 6 months, (e) 3 months, and (f) 1 month.

3.3. Trend Analysis

3.3.1. Trend Analysis at Sub-Basins Level

- For the period between 1979 and 2022

The results of the analysis indicate that there is no statistically significant evidence to suggest a change in precipitation patterns across the sub-basins in (Table 7). In fact, the p -values for each sub-basin are greater than 0.1. The observed trends vary from negative for AEHeri and Tarhat to positive for the other sub-basins. In contrast, temperature trends indicate an increase for all sub-basins, rising from 0.4 to 0.47 °C per decade. Additionally, potential evapotranspiration (PET) values increased in all sub-basins, with the greatest increase observed in the Tarhat sub-basin (40.8 mm/10 years) and the lowest in the Taghzoute sub-basin (29 mm/10 years). The trends in T and PET are highly significant, with a p -value of less than 0.01.

Table 7. Trend results for various parameters at sub-basin and Upper OER basin level (1979–2022) (***p*-value < 0.01).

1979–2022		Ahmed El Hansali	Taghzoute	Chacha N Amellah	Aval El Heri	Tarhat	Tamchachate	Upper OER
Precipitation	Z _{Mann–Kendall}	1.452	0.942	−0.188	0.544	−0.649	0.942	0.230
	Sen’s Slope	3.458	1.650	−0.529	1.456	−1.567	1.650	0.547
Temperature	Z _{Mann–Kendall}	4.812 ***	4.730 ***	5.400 ***	5.274 ***	5.358 ***	5.086 ***	5.253 ***
	Sen’s Slope	0.041 ***	0.040 ***	0.047 ***	0.045 ***	0.045 ***	0.044 ***	0.044 ***
PET	Z _{Mann–Kendall}	4.357 ***	3.747 ***	4.877 ***	4.395 ***	4.919 ***	4.899 ***	4.625 ***
	Sen’s Slope	3.936 ***	2.905 ***	3.866 ***	3.532 ***	4.083 ***	3.537 ***	3.626 ***
SPI	Z _{Mann–Kendall}	1.452	0.931	−0.188	−0.649	−0.649	−0.649	0.230
	Sen’s Slope	0.018	0.010	−0.003	−0.006	−0.006	−0.006	0.003
SPEI	Z _{Mann–Kendall}	0.238	−0.460	−1.612	−1.507	−1.507	−1.507	−1.005
	Sen’s Slope	0.004	−0.008	−0.021	−0.022	−0.022	−0.022	−0.015
RDI	Z _{Mann–Kendall}	0.954	0.544	−0.754	0.293	−0.105	−0.963	−0.126
	Sen’s Slope	0.019	0.007	−0.009	0.005	−0.002	−0.013	−0.003

With regard to the drought indices SPI, SPEI, and RDI, the trends are not significant for all sub-basins. The values for increases or decreases remain very close to 0.

- For the period between 2010 and 2022

In this period, precipitation trends indicate a significant decline across all sub-basins (Table 8). The decline in precipitation ranges from −29.2 mm/year for Taghzoute and Tamchachate to −64.6 mm/year for the Tarhat sub-basin, with a *p*-value < 0.05. During this period, temperatures exhibited an upward trend in all sub-basins. This increase is greater than that observed over the entire study period, exceeding 1 °C/10 years for AEHeri and ChachaNA, with a *p*-value of less than 0.05. The PET trends demonstrate a notable increase, with values ranging from 76.6 mm/10-years to 102.4 mm/10-years for the Tamchachate and AEH sub-basins, respectively. The observed increase is statistically significant, with a *p*-value < 0.1. The downward trends in drought indices observed in all sub-basins indicate an increase in the intensity of SPI, SPEI, and RDI. This intensity is of considerable significance, exceeding −2/10-year for four sub-basins (AEH, ChachaNA, Tarhat, and Tamchachate) for the three drought indices studied with a *p*-value of less than 0.05.

Table 8. Trend results for various parameters at sub-basin and Upper OER basin level (2010–2022) (** *p*-value < 0.05, and * *p*-value < 0.1).

2010–2022		Ahmed El Hansali	Taghzoute	Chacha N Amellah	Aval El Heri	Tarhat	Tamchachate	Upper OER
Precipitation	Z _{Mann–Kendall}	−2.400 **	−1.525	−1.769 *	−1.769 *	2.135 **	−1.525	−2.257 **
	Sen’s Slope	−48.723 **	−29.250	−38.088 *	−34.125 *	−64.666 **	−29.250	−44.835 **
Temperature	Z _{Mann–Kendall}	0.891	1.647	2.013 **	2.013 **	1.769 *	−1.525	1.891 *
	Sen’s Slope	0.047	0.092	0.106 **	0.108 **	0.077 *	0.080	0.078 *
PET	Z _{Mann–Kendall}	1.851 *	1.647	1.891 *	1.891 *	2.013 **	1.891 *	1.891 *
	Sen’s Slope	10.245 *	7.717	9.279 *	9.133 *	9.659 **	7.669 *	8.457 *
SPI	Z _{Mann–Kendall}	−2.400 **	−1.525	−1.769 *	−2.135 **	−2.135 **	−2.135 **	−2.257 **
	Sen’s Slope	−0.228 **	−0.144	−0.165 *	−0.225 **	−0.225 **	−0.225 **	−0.224 **
SPEI	Z _{Mann–Kendall}	−2.537 **	−1.891 *	−2.257 **	−2.501 **	−2.501 **	−2.501 **	−2.501 **
	Sen’s Slope	−0.249 **	−0.188 *	−0.200 **	−0.205 **	−0.205 **	−0.205 **	−0.246 **
RDI	Z _{Mann–Kendall}	−2.263 **	−1.647	−1.891 *	−2.013 **	−2.135 **	−2.257 **	−2.379 **
	Sen’s Slope	−0.245 **	−0.152	−0.169 *	−0.202 **	−0.172 **	−0.221 **	−0.234 **

3.3.2. Trend Analysis at Upper OER Watershed Level

As shown in (Table 7), over the study period (44 years), precipitation (P), mean temperature (Tmean), and potential evapotranspiration (PET) show an upward trend, with 5 mm/10-year, 0.4 °C/10-year and 36.2 mm/10-year, respectively. This trend is not statistically significant for precipitation, with a *p*-value greater than 0.1, in contrast to what is found for Tmean and PET, with a *p*-value less than 0.01. The analysis of drought indices revealed an increasing trend for SPI and a decreasing trend for SPEI and RDI. However, these trends remain insignificant given the very high *p*-value.

For the period 2010–2022 (Table 8), all trends are statistically significant. Precipitation exhibits an interesting downward trend with a rate of −44.8 mm/year, which is statistically significant at the 0.05 level. In contrast, Tmean and PET show upward trends with rates of 0.78 °C/10-year and 84.5 mm/10-year, respectively, which are statistically significant, with a *p*-value less than 0.1. The SPI, SPEI, and RDI indices demonstrate a declining trend within the Upper Oum Er Rbia watershed. The intensity of drought is −2.24/10-year, −2.47/10-year, and −2.35/10-year, respectively, with a *p*-value <0.05 for SPI, SPEI, and RDI.

4. Discussion

In this study, we integrated multiple datasets and analytical techniques that, to the best of our knowledge, have never been concurrently used in a study in Morocco. The objective was to obtain a comprehensive and detailed understanding of the evolution of drought in Morocco, especially in mountainous area, with the Upper Oum Er Rbia basin serving as a case study.

In this investigation, actual precipitation data were used, whereas temperature data were derived from the European Centre for Medium-Range Weather Forecasts (ECMWF) Reanalysis (ERA5) dataset. The correlation between these datasets and the two stations with data available was very good. The results of this study may prove useful in the future, where measuring stations are absent, and further research may be conducted in this area.

In order to analyze the drought conditions in the Upper Oum Er Rbia watershed, a series of indices were applied, namely SPI (Standard Precipitation Index), SPEI (Standardized Precipitation Evapotranspiration Index), and RDI (Reconnaissance Drought Index). However, drought indices have been demonstrated to be highly effective tools for monitoring and tracking drought, due to their capacity to simplify the complex interactions between diverse climatic parameters [110].

The indices demonstrate that the duration of drought varies between sub-basins and according to the chosen time step. Tamchachate exhibited the longest duration of drought at the 1-month time step, with 96 months. With a three-month time step, Taghzoute and Tamchachate exhibited the greatest degree of drought impact, with 145 and 143 months, respectively. With a duration of 159 months, AEHeri is the sub-basin that has experienced the longest period of drought with the 6-month time step. The sub-basin most affected by drought with a duration of 160 months by the 12-month time step is AEHansali. Conversely, the sub-basin that experienced the shortest duration of drought is ChachaNA. In all the sub-basins studied and with the different drought indices (SPI, SPEI, and RDI), the three-month time step shows the highest number of months with high drought intensity (extreme drought), indicating that the three-month time step is the most sensitive to drought.

In all of the sub-basins under examination, and with various drought indices (SPI, SPEI, and RDI), the three-month time step consistently showed the highest number of months with high drought intensity (extreme drought). The result of this analysis indicates that the three-month time step is particularly sensitive in detecting drought conditions. The frequent occurrence of extreme droughts during this time step highlights its effectiveness in capturing short-term variations in water availability and stress.

The results of the correlation between the various drought indices SPI, SPEI, RDI, NDVI, EVI, and CWSI and precipitation were carried out for all sub-basins. The analysis demonstrated that the best correlation between drought indices was that between RDI and SPI for the different time steps and at the level of the majority of sub-basins. Pre-

precipitation exhibited a stronger correlation with SPEI and RDI at the 1-month time step, yet the most notable correlation was that between precipitation and CWSI. At the annual time step, the correlation between precipitation and the SPI, SPEI, and RDI indices was particularly noteworthy.

In the majority of the sub-basins under investigation, the Standardized Precipitation Evapotranspiration Index (SPEI) with a time step of six months exhibits the most pronounced correlation with the two vegetation indices, namely the Normalized Difference Vegetation Index (NDVI) and the Enhanced Vegetation Index (EVI). This observation is in alignment with the research findings presented by [111]. However, it is noteworthy that this correlation is generally categorized as weak. This pattern is mirrored in the research conducted by [67], who reported similar results in the mountainous regions of their study area. This region, which is located to the southwest of our basin, is characterized by a subhumid climate and is composed of forests, dry grazing areas, and shrubs. The Upper OER basin, which is also located at high altitudes and is predominantly forested, shows an exception in the AEHansali sub-basin. Here, the highest correlation values were 0.437 and 0.389 between SPEI and NDVI and between SPEI and EVI, respectively, indicating a moderate-to-weak positive relationship.

In the study of drought indices and their relationship with the Crop Water Stress Index (CWSI), it has been observed that the strongest correlation exists between the CWSI and the Standardized Precipitation Evapotranspiration Index (SPEI). This correlation is akin to the one observed between the Normalized Difference Vegetation Index (NDVI) and the Enhanced Vegetation Index (EVI). However, correlation coefficients are a notable distinction. While CWSI and SPEI showed a moderate correlation in all sub-basins, the correlation coefficients ranged from 0.472 to 0.504. These results demonstrated an improvement when compared with those obtained with NDVI and EVI. The analysis revealed that the highest correlation was identified in the AEH sub-basin. It is noteworthy that this correlation was observed with a temporal resolution of three months, differing from the results obtained previously. When the analysis was extended to an annual time step, encompassing all sub-basins and drought indices, the correlation was found to be strong to very strong. This suggests a robust relationship between these variables over an extended period.

It must be noted that this study used remote-sensing products, which have limited applicability across all geographical terrains. It is noteworthy that regions with mountainous topography present unique challenges. However, the AEHansali sub-basin has shown optimal results. This can be attributed to its relatively minimal altitude variance in comparison to other sub-basins.

Consequently, a comprehensive analysis of the correlation results at the sub-basin level was required in order to examine the relationships between these indices, with a particular focus on seasonal variations. The spring season demonstrated the most favorable outcomes, as evidenced by the correlations between SPEI/NDVI, SPEI/EVI, and SPEI/CWSI, which were 0.739, 0.746, and 0.821, respectively. These results were statistically significant, with a p -value of less than 0.001, indicating a high level of confidence in the findings. The analysis demonstrated an improvement in the ability of remote-sensing indexes to accurately capture drought conditions.

The integration of Mann–Kendall and Sen’s Slope for the study of trends is a particularly interesting approach, as it helps to understand the temporal evolution of the different parameters used in this study.

The analysis of precipitation at the sub-basin level for the period 1979–2022 revealed a decreasing trend at Tarhat and ChachaNA, while an increasing trend was observed at other sub-basins. These trends, whether increasing or decreasing, remain unrepresentative due to the p -value exceeding 0.1. The observed increase in precipitation in some sub-basins is likely due to the presence of positive precipitation anomalies recorded in 1995–1996 and 2009–2010 in most regions of Morocco, as reported by [62].

As the temperature showed an increasing trend, with a p -value less than 0.01, in the six sub-basins, the rise in temperature was noticeable, with an increase between

0.4 °C/10 years and 0.47 °C/10 years at the level of the Taghzoute and ChachaNA sub-basins, respectively. The same results were observed for the trends of potential evapotranspiration, where an increase was noted for all the sub-basins. The magnitude of this increase varied between 29.05 mm/10 years and 40.83 mm/10 years for Taghzoute and Tarhat, respectively.

Similarly, at the level of the Haut Oum Er Rbia basin, an increase in temperature and potential evapotranspiration (PET) was observed, with 0.44 °C/10 and 36.26 mm/10 years, respectively, with a *p*-value less than 0.01. Conversely, precipitation and drought indices did not reveal any significant trends for this period.

Nevertheless, despite the availability of remote-sensing data from the year 2000 onward, it was imperative for this study to analyze the trends of different parameters from the hydrological year 2010–2011 onward, in order to avoid any confusion resulting from the anomaly of 2009–2010.

In contrast to the preceding period, the trends of the various parameters during the period 2010–2022 are statistically significant for the majority of them.

All sub-basins are suffering from a very significant lack of precipitation; during the last 13 years, precipitation has been strongly decreasing at all sub-basin levels, with a decrease varying from −29.25 mm/year in Taghzoute to −64.66 mm/year in Tarhat.

The temperature trend in this period is more pronounced than in the period 1979–2022. The sub-basins most affected by the increase in temperature are ChachaNA 1.08 °C/10 years and AEHeri 1.06 °C/10 years.

PET is also on the rise, as precipitation has decreased, and temperature has increased; the sub-basins that show the highest value of trends are AEH 102.45 mm/10 years and Tarhat 96.59 mm/10 years.

All drought indices are demonstrating a downward trend, exceeding −0.2 per year, which is a significant indicator. These indices serve as essential tools for assessing the impact of drought on water resources. Upon closer examination, we find that the AEH sub-basin has the lowest values for the drought indices SPI, SPEI, and RDI, with −0.228 per year, −0.249 per year, and −0.245 per year, respectively. This indicates that this region is particularly affected by drought. In contrast, the Taghzoute sub-basin shows less severe values, with −0.144 per year for SPI, −0.188 per year for SPEI, and −0.152 per year for RDI. Indeed, among the sub-basins under discussion, Taghzoute is the least affected by drought.

From an overall perspective, the Upper Oum Er Rbia basin has experienced a notable shift in climatic patterns. A decrease in precipitation of −44.835 mm/year has been observed, indicating a trend toward drier conditions. Concurrently, both temperature and potential evapotranspiration have shown an increase, with a rate of 0.78 °C per decade and 84.57 mm per decade, respectively. This indicates a warming trend and an increase in the potential for water loss from the land to the atmosphere. Furthermore, the drought indices demonstrate a decreasing trend, with SPI, SPEI, and RDI at −0.224/year, −0.246/year, and −0.234/year, respectively. These indices are used to quantify the severity and duration of drought conditions. A negative trend indicates a worsening of drought conditions over time.

These changes have significant implications for the management of water resources in the Haut Oum Er Rbia basin. The observed decrease in precipitation and concurrent increase in temperature and potential evapotranspiration indicate that water availability may become relatively more limited in the future. The negative trends observed in the drought indices serve to reinforce the conclusion that drought conditions are becoming increasingly severe.

Previous studies suggest that integrating river-flow data is an effective method for evaluating the impact of watershed disturbances on hydrological drought conditions [112–114]. Incorporating river-flow data into future research could provide a more nuanced understanding of hydrological droughts. Combining these results with current findings will provide a complete vision of environmental drought, encompassing meteorological, hydrological, and agricultural aspects.

Adaptation strategies will be needed to manage water resources under these changing climate conditions. This could include measures to increase water-use efficiency, develop alternative water sources, and implement sustainable land-management practices to reduce evapotranspiration and conserve soil moisture. It is also important to monitor these climate and drought indices regularly to track changes over time and adjust management strategies as needed.

5. Conclusions

The findings of this study underscore the importance of the three-month time step as a crucial interval for monitoring and evaluating drought conditions, providing essential insights for effective water resource management and strategic planning. Among the various indices analyzed, the Standardized Precipitation Evapotranspiration Index (SPEI) emerges as the optimal choice for integration with remote-sensing products, offering a comprehensive assessment of drought by accounting for both precipitation and evapotranspiration. Notably, the Crop Water Stress Index (CWSI) demonstrates a strong correlation with SPEI at the three-month scale, surpassing the performance of NDVI and EVI. Seasonal trends indicate that agricultural indices, particularly during the spring, align more closely with meteorological indices, with CWSI maintaining the highest consistency in correlation with SPEI-3. Furthermore, the analysis of climate trends from 2010 to 2022 reveals a significant decrease in precipitation, alongside increasing temperatures and evapotranspiration potential (ETP), which exacerbate drought conditions in the study area. Consequently, all indices—including SPI, SPEI, and RDI—indicate an increase in drought intensity, highlighting the urgent need for adaptive strategies to manage water resources effectively in light of these changing climatic conditions.

Author Contributions: Conceptualization, M.M.M.; Methodology, A.Z.; Formal analysis, M.M.M. and A.Z.; Writing—original draft, M.M.M. and E.-I.K.; Writing—review & editing, Y.A.B., M.A. and O.T.; Supervision, L.B. and M.A.; Funding acquisition, Y.A.B. All authors have read and agreed to the published version of the manuscript.

Funding: This research received no external funding.

Data Availability Statement: The data that support the findings of this study are available from the corresponding author upon reasonable request.

Conflicts of Interest: The authors declare no conflict of interest.

References

1. Ndayiragije, J.M.; Li, F. Monitoring and Analysis of Drought Characteristics Based on Climate Change in Burundi Using Standardized Precipitation Evapotranspiration Index. *Water* **2022**, *14*, 2511. [CrossRef]
2. United Nations Office for Disaster Risk Reduction (UNDRR). Special Report on Drought 2021. 2021. Available online: <https://www.undrr.org/publication/gar-special-report-drought-2021> (accessed on 12 March 2023).
3. Bageshree, K.; Abhishek; Kinouchi, T. A Multivariate Drought Index for Seasonal Agriculture Drought Classification in Semiarid Regions. *Remote Sens.* **2022**, *14*, 3891. [CrossRef]
4. Lloyd-Hughes, B. The Impracticality of a Universal Drought Definition. *Theor. Appl. Climatol.* **2014**, *117*, 607–611. [CrossRef]
5. Tate, E.L.; Gustard, A. Drought Definition: A Hydrological Perspective. In *Drought and Drought Mitigation in Europe*; Springer: Dordrecht, The Netherlands, 2000; pp. 23–48. [CrossRef]
6. World Meteorological Organization. Drought. Available online: <https://wmo.int/about-us/world-meteorological-day/wmd-2020/drought> (accessed on 3 February 2023).
7. Cao, S.; Zhang, L.; He, Y.; Zhang, Y.; Chen, Y.; Yao, S.; Yang, W.; Sun, Q. Effects and Contributions of Meteorological Drought on Agricultural Drought under Different Climatic Zones and Vegetation Types in Northwest China. *Sci. Total Environ.* **2022**, *821*, 153270. [CrossRef] [PubMed]
8. Trenberth, K.E.; Dai, A.; Van Der Schrier, G.; Jones, P.D.; Barichivich, J.; Briffa, K.R.; Sheffield, J. Global Warming and Changes in Drought. *Nat. Clim. Chang.* **2014**, *4*, 17–22. [CrossRef]
9. Benzougagh, B.; Meshram, S.G.; Baamar, B.; Dridri, A.; Boudad, L.; Sadkaoui, D.; Mimich, K. Relationship between Landslide and Morpho-Structural Analysis: A Case Study in Northeast of Morocco. *Appl. Water Sci.* **2020**, *10*, 175. [CrossRef]

10. Benzougagh, B.; Meshram, S.G.; El Fellah, B.; Mastere, M.; Dridri, A.; Sadkaoui, D.; Mimich, K.; Khedher, K.M. Combined Use of Sentinel-2 and Landsat-8 to Monitor Water Surface Area and Evaluated Drought Risk Severity Using Google Earth Engine. *Earth Sci. Inform.* **2022**, *15*, 929–940. [[CrossRef](#)]
11. Tigkas, D.; Vangelis, H.; Tsakiris, G. Drought and Climatic Change Impact on Streamflow in Small Watersheds. *Sci. Total Environ.* **2012**, *440*, 33–41. [[CrossRef](#)]
12. Zhou, Z.; Shi, H.; Fu, Q.; Ding, Y.; Li, T.; Wang, Y.; Liu, S. Characteristics of Propagation from Meteorological Drought to Hydrological Drought in the Pearl River Basin. *J. Geophys. Res. Atmos.* **2021**, *126*, e2020JD033959. [[CrossRef](#)]
13. Angelidis, P.; Maris, F.; Kotsovinos, N.; Hrisanthou, V. Computation of Drought Index SPI with Alternative Distribution Functions. *Water Resour. Manag.* **2012**, *26*, 2453–2473. [[CrossRef](#)]
14. WMO. Available online: <https://wmo.int/media/news/droughts-threaten-sustainable-development> (accessed on 3 February 2023).
15. NDMC. 2022. Available online: <https://drought.unl.edu/Education/DroughtforKids/DroughtEffects.aspx> (accessed on 3 February 2023).
16. Ionita, M.; Scholz, P.; Chelcea, S. Assessment of Droughts in Romania Using the Standardized Precipitation Index. *Nat. Hazards* **2016**, *81*, 1483–1498. [[CrossRef](#)]
17. Wu, J.; Zhou, L.; Mo, X.; Zhou, H.; Zhang, J.; Jia, R. Drought Monitoring and Analysis in China Based on the Integrated Surface Drought Index (ISDI). *Int. J. Appl. Earth Obs. Geoinf.* **2015**, *41*, 23–33. [[CrossRef](#)]
18. Nkuzimana, A.; Shuoben, B.; Guojie, W.; Alriah, M.A.A.; Sarfo, I.; Zhihui, X.; Vuguziga, F.; Ayugi, B.O. Assessment of Drought Events, Their Trend and Teleconnection Factors over Burundi, East Africa. *Theor. Appl. Climatol.* **2021**, *145*, 1293–1316. [[CrossRef](#)]
19. Park, S.; Im, J.; Park, S.; Rhee, J. Drought Monitoring Using High Resolution Soil Moisture through Multi-Sensor Satellite Data Fusion over the Korean Peninsula. *Agric. For. Meteorol.* **2017**, *237–238*, 257–269. [[CrossRef](#)]
20. Anderegg, W.R.L.; Kane, J.M.; Anderegg, L.D.L. Consequences of Widespread Tree Mortality Triggered by Drought and Temperature Stress. *Nat. Clim. Chang.* **2013**, *3*, 30–36. [[CrossRef](#)]
21. Nepstad, D.C.; Tohver, I.M.; Ray, D.; Moutinho, P.; Ecology, S.; Sep, N.; Nepstad, C. Mortality of Large Trees and Lianas Following Experimental Drought in an Amazon Forest. *Ecology* **2015**, *88*, 2259–2269. [[CrossRef](#)]
22. da Silva, S.S.; Fearnside, P.M.; de Alencastro Graça, P.M.L.; Brown, I.F.; Alencar, A.; de Melo, A.W.F. Dynamics of Forest Fires in the Southwestern Amazon. *For. Ecol. Manag.* **2018**, *424*, 312–322. [[CrossRef](#)]
23. Liu, C.; Yang, C.; Yang, Q.; Wang, J. Spatiotemporal Drought Analysis by the Standardized Precipitation Index (SPI) and Standardized Precipitation Evapotranspiration Index (SPEI) in Sichuan Province, China. *Sci. Rep.* **2021**, *11*, 1280. [[CrossRef](#)]
24. Zribi, M.; Dridi, G.; Amri, R.; Lili-Chabaane, Z. Analysis of the Effects of Drought on Vegetation Cover in a Mediterranean Region through the Use of SPOT-VGT and TERRA-MODIS Long Time Series. *Remote Sens.* **2016**, *8*, 992. [[CrossRef](#)]
25. The Food and Agriculture Organization of the United Nations. *The Impact of Disasters and Crises on Agriculture and Food Security: 2021*; FAO: Rome, Italy, 2021; ISBN 978-92-5-134071-4.
26. Wu, B.; Ma, Z.; Yan, N. Agricultural Drought Mitigating Indices Derived from the Changes in Drought Characteristics. *Remote Sens. Environ.* **2020**, *244*, 111813. [[CrossRef](#)]
27. Winkler, K.; Gessner, U.; Hochschild, V. Identifying Droughts Affecting Agriculture in Africa Based on Remote Sensing Time Series between 2000–2016: Rainfall Anomalies and Vegetation Condition in the Context of ENSO. *Remote Sens.* **2017**, *9*, 831. [[CrossRef](#)]
28. West, H.; Quinn, N.; Horswell, M. Remote Sensing for Drought Monitoring & Impact Assessment: Progress, Past Challenges and Future Opportunities. *Remote Sens. Environ.* **2019**, *232*, 111291. [[CrossRef](#)]
29. Wilhite, D.A.; Glantz, M.H. Understanding: The Drought Phenomenon: The Role of Definitions. *Water Int.* **1985**, *10*, 111–120. [[CrossRef](#)]
30. Crausbay, S.D.; Ramirez, A.R.; Carter, S.L.; Cross, M.S.; Hall, K.R.; Bathke, D.J.; Betancourt, J.L.; Colt, S.; Cravens, A.E.; Dalton, M.S.; et al. Defining Ecological Drought for the Twenty-First Century. *Bull. Am. Meteorol. Soc.* **2017**, *98*, 2543–2550. [[CrossRef](#)]
31. Bradford, J.B.; Schlaepfer, D.R.; Palmquist, K.A.; Lauenroth, W.K. Robust Ecological Drought Projections for Drylands in the 21st Century. *Glob. Chang. Biol.* **2020**, *26*, 3906–3919. [[CrossRef](#)]
32. Christian, J.I.; Basara, J.B.; Otkin, J.A.; Hunt, E.D.; Wakefield, R.A.; Flanagan, P.X.; Xiao, X. A Methodology for Flash Drought Identification: Application of Flash Drought Frequency across the United States. *J. Hydrometeorol.* **2019**, *20*, 833–846. [[CrossRef](#)]
33. Hu, C.; Xia, J.; She, D.; Li, L.; Song, Z.; Hong, S. A New Framework for the Identification of Flash Drought: Multivariable and Probabilistic Statistic Perspectives: Identification of Flash Drought. *Int. J. Climatol.* **2021**, *41*, 5862–5878. [[CrossRef](#)]
34. Son, B.; Park, S.; Im, J.; Park, S.; Ke, Y.; Quackenbush, L.J. Remote Sensing of Environment A New Drought Monitoring Approach: Vector Projection Analysis (VPA). *Remote Sens. Environ.* **2021**, *252*, 112145. [[CrossRef](#)]
35. Ha, T.V.; Huth, J.; Bachofer, F.; Kuenzer, C. A Review of Earth Observation-Based Drought Studies in Southeast Asia. *Remote Sens.* **2022**, *14*, 3763. [[CrossRef](#)]
36. McKee, T.B.; Nolan, J.; Kleist, J. The relationship of drought frequency and duration to time scales. In Proceedings of the 8th Conference on Applied Climatology, Anaheim, CA, USA, 17–22 January 1993.
37. Bhalme, H.N.; Mooley, D.A. Large-Scale Droughts/ Floods and Monsoon Circulation. *Mon. Weather Rev.* **1980**, *108*, 1197–1211. [[CrossRef](#)]
38. Tsakiris, G.; Vangelis, H. Establishing a Drought Index Incorporating Evapotranspiration. *Eur. Water* **2005**, *9*, 3–11.

39. Palmer, W.C. *Meteorological Drought*; Research Paper No. 45; US Department of Commerce, Weather Bureau: Washington, DC, USA, 1965; p. 58.
40. Vicente-Serrano, S.M.; Beguería, S.; López-Moreno, J.I. A Multiscalar Drought Index Sensitive to Global Warming: The Standardized Precipitation Evapotranspiration Index. *J. Clim.* **2010**, *23*, 1696–1718. [[CrossRef](#)]
41. Narasimhan, B.; Srinivasan, R. Development and Evaluation of Soil Moisture Deficit Index (SMDI) and Evapotranspiration Deficit Index (ETDI) for Agricultural Drought Monitoring. *Agric. For. Meteorol.* **2005**, *133*, 69–88. [[CrossRef](#)]
42. British Columbia | Ministry of Agriculture. Soil Water Storage Capacity and Available Soil Moisture. *Water Conserv. Factsheet* **2015**, *1*, 1–4.
43. Nalbantis, I.; Tsakiris, G. Assessment of Hydrological Drought Revisited. *Water Resour. Manag.* **2009**, *23*, 881–897. [[CrossRef](#)]
44. Staudinger, M.; Stahl, K.; Seibert, J. A Drought Index Accounting for Snow. *Water Resour. Res.* **2014**, *50*, 7861–7872. [[CrossRef](#)]
45. Huete, A.; Didan, K.; Miura, T.; Rodriguez, E.P.; Gao, X.; Ferreira, L.G. Overview of the Radiometric and Biophysical Performance of the MODIS Vegetation Indices. *Remote Sens. Environ.* **2002**, *83*, 195–213. [[CrossRef](#)]
46. Kogan, F.N. Droughts of the Late 1980s in the United States as Derived from NOAA Polar-Orbiting Satellite Data. *Bull.-Am. Meteorol. Soc.* **1995**, *76*, 655–668. [[CrossRef](#)]
47. Tarpley, J.D.; Schneider, S.R.; Money, R.L. Global Vegetation Indices from the NOAA-7 Meteorological Satellite. *J. Clim. Appl. Meteorol.* **1984**, *23*, 491–494. [[CrossRef](#)]
48. Brown, J.F.; Wardlow, B.D.; Tadesse, T.; Hayes, M.J.; Reed, B.C. The Vegetation Drought Response Index (VegDRI): A New Integrated Approach for Monitoring Drought Stress in Vegetation. *Glsci Remote Sens.* **2008**, *45*, 16–46. [[CrossRef](#)]
49. Hao, Z.; AghaKouchak, A.; Nakhjiri, N.; Farahmand, A. Global Integrated Drought Monitoring and Prediction System. *Sci. Data* **2014**, *1*, 140001. [[CrossRef](#)] [[PubMed](#)]
50. Rodell, M.; Houser, P.R.; Jambor, U.; Gottschalck, J.; Mitchell, K.; Meng, C.J.; Arsenault, K.; Cosgrove, B.; Radakovich, J.; Bosilovich, M.; et al. The Global Land Data Assimilation System. *Bull. Am. Meteorol. Soc.* **2004**, *85*, 381–394. [[CrossRef](#)]
51. Svoboda, M.; LeComte, D.; Hayes, M.; Heim, R.; Gleason, K.; Angel, J.; Rippey, B.; Tinker, R.; Palecki, M.; Stooksbury, D.; et al. The Drought Monitor. *Bull. Am. Meteorol. Soc.* **2002**, *83*, 1181–1190. [[CrossRef](#)]
52. Mann, H.B. Non-Parametric Test Against Trend. *Econometrica* **1945**, *13*, 245–259. [[CrossRef](#)]
53. Kendall, M.G. *Rank Correlation Methods*, 4th ed.; Griffin: London, UK, 1975; ISBN 0852641990; 9780852641996.
54. Sen, P.K. Estimates of the Regression Coefficient Based on Kendall's Tau. *J. Am. Stat. Assoc.* **1968**, *63*, 1379–1389. [[CrossRef](#)]
55. Caloiero, T.; Veltri, S.; Caloiero, P.; Frustaci, F. Drought Analysis in Europe and in the Mediterranean Basin Using the Standardized Precipitation Index. *Water* **2018**, *10*, 1043. [[CrossRef](#)]
56. Bijaber, N.; El Hadani, D.; Saidi, M.; Svoboda, M.D.; Wardlow, B.D.; Hain, C.R.; Poulsen, C.C.; Yesséf, M.; Rochdi, A. Developing a Remotely Sensed Drought Monitoring Indicator for Morocco. *Geosciences* **2018**, *8*, 55. [[CrossRef](#)]
57. Bouras, E.; Jarlan, L.; Er-raki, S. Linkages between Rainfed Cereal Production and Agricultural Drought through Remote Sensing Indices and a Land Data Assimilation System: A Case Study in Morocco. *Remote Sens.* **2020**, *12*, 4018. [[CrossRef](#)]
58. Hachem, A.; Mili, E.; Benbella, B.; El Ouardi, H.; Mehdaoui, R. Characterization of Climatic Drought Sequences in the Upper Moulouya Watershed, Morocco. *Ecol. Eng. Environ. Technol.* **2023**, *24*, 162–179. [[CrossRef](#)]
59. Ayad, N.A.; Ayad, A.A.; El Khalidi, K.; Habib, A.; Charif, A. Remote Sensing and Meteorological Indexes of Drought Using Open Short Time-Series Data in Doukkala Region, Morocco. *Ecol. Eng. Environ. Technol.* **2023**, *24*, 1–10. [[CrossRef](#)]
60. Bounoua, I.; Saidi, Y.; Yaagoubi, R.; Bouziani, M. Deep Learning Approaches for Water Stress Forecasting in Arboriculture Using Time Series of Remote Sensing Images: Comparative Study between ConvLSTM and CNN-LSTM Models. *Technologies* **2024**, *12*, 77. [[CrossRef](#)]
61. Najmi, A.; Igmoullan, B.; Namous, M.; El Bouazzaoui, I.; Brahim, Y.A.; El Khalki, E.M.; Saidi, M.E.M. Evaluation of PERSIANN-CCS-CDR, ERA5, and SM2RAIN-ASCAT Rainfall Products for Rainfall and Drought Assessment in a Semi-Arid Watershed, Morocco. *J. Water Clim. Chang.* **2023**, *14*, 1569–1584. [[CrossRef](#)]
62. Ouatiki, H.; Boudhar, A.; Ouhinou, A.; Arioua, A.; Hssaisoune, M. Trend Analysis of Rainfall and Drought over the Oum Er-Rbia River Basin in Morocco during 1970–2010. *Arab. J. Geosci.* **2019**, *12*, 128. [[CrossRef](#)]
63. Kessabi, R.; Hanchane, M.; Krakauer, N.Y.; Aboubi, I.; El Kassioui, J.; El Khazzan, B. Annual, Seasonal, and Monthly Rainfall Trend Analysis through Non-Parametric Tests in the Sebou River Basin (SRB), Northern Morocco. *Climate* **2022**, *10*, 170. [[CrossRef](#)]
64. Kessabi, R.; Hanchane, M.; Guijarro, J.A.; Krakauer, N.Y.; Addou, R.; Sadiki, A.; Belmahi, M. Homogenization and Trends Analysis of Monthly Precipitation Series in the Fez-Meknes Region, Morocco. *Climate* **2022**, *10*, 64. [[CrossRef](#)]
65. Hadri, A.; El, M.; Saidi, M.; Boudhar, A. Multiscale Drought Monitoring and Comparison Using Remote Sensing in a Mediterranean Arid Region: A Case Study from West-Central Morocco. *Arab. J. Geosci.* **2021**, *14*, 118. [[CrossRef](#)]
66. Kessabi, R.; Hanchane, M.; Caloiero, T.; Pellicone, G.; Addou, R.; Krakauer, N.Y. Analyzing Spatial Trends of Precipitation Using Gridded Data in the Fez-Meknes Region, Morocco. *Hydrology* **2023**, *10*, 37. [[CrossRef](#)]
67. Hakam, O.; Baali, A.; Ait Brahim, Y.; El Kamel, T.; Azennoud, K. Regional and Global Teleconnections Patterns Governing Rainfall in the Western Mediterranean: Case of the Lower Sebou Basin, North-West Morocco. *Model. Earth Syst. Environ.* **2022**, *8*, 5107–5128. [[CrossRef](#)]
68. Khalil, N.; Rouane, S.E.; Mania, J.; Murdry, J. Sur Les Eaux Du Haut Bassin (Moyen Atlas, Maroc) Hydrochimical Balance Assessment in the High Basin of the Oum Er Rbia. *Rev. Fr. Geotech.* **2004**, 75–85. [[CrossRef](#)]

69. El Jihad, M. Les Difficultés de Gestion Des Ressources «naturelles» et de Développement Rural Dans Un Milieu Anthropisé: L'expérience Du Projet Oued Srou (Maroc Central). *Noréis* **2010**, *3*, 25–45. [CrossRef]
70. Rhoujjati, N.; Ait Brahim, Y.; Hanich, L.; Rhoujjati, A.; Rafik, A.; Ouatiki, H.; Chehbouni, A.; Bouchaou, L. Snowpack and Groundwater Recharge in the Atlas Mountains: New Evidence and Key Drivers. *J. Hydrol. Reg. Stud.* **2023**, *49*, 101520. [CrossRef]
71. OERHBA Agency. Oum Er Rbia Water Basin. OERHBA Oum Er Rbia Hydraulic Basin Agency. Available online: <http://www.abhoer.ma/> (accessed on 30 March 2023).
72. C3S Copernicus Climate Change Service, Climate Data Store: ERA5 Hourly Data on Pressure Levels from 1940 to Present. Available online: <https://cds.climate.copernicus.eu/cdsapp#!/dataset/reanalysis-era5-pressure-levels?tab=overview> (accessed on 18 February 2023).
73. Hersbach, H.; Bell, B.; Berrisford, P.; Hirahara, S.; Horányi, A.; Muñoz-Sabater, J.; Nicolas, J.; Peubey, C.; Radu, R.; Schepers, D.; et al. The ERA5 Global Reanalysis. *Q. J. R. Meteorol. Soc.* **2020**, *146*, 1999–2049. [CrossRef]
74. Dee, D.P.; Uppala, S.M.; Simmons, A.J.; Berrisford, P.; Poli, P.; Kobayashi, S.; Andrae, U.; Balmaseda, M.A.; Balsamo, G.; Bauer, P.; et al. The ERA-Interim Reanalysis: Configuration and Performance of the Data Assimilation System. *Q. J. R. Meteorol. Soc.* **2011**, *137*, 553–597. [CrossRef]
75. Uppala, S.M.; Kållberg, P.W.; Simmons, A.J.; Andrae, U.; Bechtold, V.D.C.; Fiorino, M.; Gibson, J.K.; Haseler, J.; Hernandez, A.; Kelly, G.A.; et al. The ERA-40 Re-Analysis. *Q. J. R. Meteorol. Soc.* **2005**, *131*, 2961–3012. [CrossRef]
76. Gibson, J.K.; Kållberg, P.; Uppala, S.; Hernandez, A.; Nomura, A.; Serrano, E. ERA-15 Description. ECMWF Re-Analysis Project Report Series, No. 1, Version 2. 1999. Available online: <https://www.ecmwf.int/sites/default/files/elibrary/1997/9584-era-description.pdf> (accessed on 30 March 2023).
77. Bengtsson, L.; Kanamitsu, M.; Kållberg, P.; Uppala, S. FGGE Research Activities at ECMWF. *Bull. Am. Meteorol. Soc.* **1982**, *63*, 277–303. [CrossRef]
78. Li, L.; She, D.; Zheng, H.; Lin, P.; Yang, Z.-L. Elucidating Diverse Drought Characteristics from Two Meteorological Drought Indices (SPI and SPEI) in China. *J. Hydrometeorol.* **2020**, *21*, 1513–1530. [CrossRef]
79. Vicente-Serrano, S.M. Differences in Spatial Patterns of Drought on Different Time Scales: An Analysis of the Iberian Peninsula. *Water Resour. Manag.* **2006**, *20*, 37–60. [CrossRef]
80. Hayes, M.; Svoboda, M.; Wall, N.; Widhalm, M. The Lincoln Declaration on Drought Indices: Universal Meteorological Drought Index Recommended. *Bull. Am. Meteorol. Soc.* **2011**, *92*, 485–488. [CrossRef]
81. Capra, A.; Scicolone, B. Spatiotemporal Variability of Drought on a Short-Medium Time Scale in the Calabria Region (Southern Italy). *Theor. Appl. Climatol.* **2012**, *110*, 471–488. [CrossRef]
82. Svoboda, M.D.; Fuchs, B.A. *Handbook of Drought Indicators and Indices*; World Meteorological Organization: Geneva, Switzerland, 2016; Volume 1173.
83. Tigkas, D.; Vangelis, H.; Tsakiris, G. An Enhanced Effective Reconnaissance Drought Index for the Characterisation of Agricultural Drought. *Environ. Process.* **2017**, *4*, S137–S148. [CrossRef]
84. An, S.; Park, G.; Jung, H.; Jang, D. Assessment of Future Drought Index Using SSP Scenario in Rep. of Korea. *Sustainability* **2022**, *14*, 4252. [CrossRef]
85. Mohammed, Y.; Yimam, A. Analysis of Meteorological Droughts in the Lake's Region of Ethiopian Rift Valley Using Reconnaissance Drought Index (RDI). *Geoenvirom. Disasters* **2021**, *8*, 13. [CrossRef]
86. Ren, Y.; Liu, J.; Shalamzari, M.J.; Arshad, A.; Liu, S.; Liu, T.; Tao, H. Monitoring Recent Changes in Drought and Wetness in the Source Region of the Yellow River Basin, China. *Water* **2022**, *14*, 861. [CrossRef]
87. Ogunrinde, A.T.; Oguntunde, P.G.; Akinwumiju, A.S.; Fasinmirin, J.T.; Adawa, I.S.; Ajayi, T.A. Effects of Climate Change and Drought Attributes in Nigeria Based on RCP 8.5 Climate Scenario. *Phys. Chem. Earth* **2023**, *129*, 103339. [CrossRef]
88. Guttman, N.B. On the Sensitivity of Sample L Moments to Sample Size. *J. Clim.* **1994**, *7*, 1026–1029. [CrossRef]
89. Tigkas, D.; Vangelis, H.; Tsakiris, G. DrinC: A Software for Drought Analysis Based on Drought Indices. *Earth Sci. Inform.* **2015**, *8*, 697–709. [CrossRef]
90. Aiguo, D.; Kevin, E.T.; Taotao, Q. A Global Dataset of Palmer Drought Severity Index for 1870–2002: Relationship with Soil Moisture and Effects of Surface Warming. *J. Hydrometeorol.* **2004**, *5*, 1117–1130.
91. Zarei, A.R.; Moghimi, M.M.; Bahrami, M. Comparison of Reconnaissance Drought Index (RDI) and Effective Reconnaissance Drought Index (ERDI) to Evaluate Drought Severity. *Sustain. Water Resour. Manag.* **2019**, *5*, 1345–1356. [CrossRef]
92. Zhang, F.; Zhou, G. Estimation of Vegetation Water Content Using Hyperspectral Vegetation Indices: A Comparison of Crop Water Indicators in Response to Water Stress Treatments for Summer Maize. *BMC Ecol.* **2019**, *19*, 18. [CrossRef]
93. Cao, Z.; Wang, Q.; Zheng, C. Best Hyperspectral Indices for Tracing Leaf Water Status as Determined from Leaf Dehydration Experiments. *Ecol. Indic.* **2015**, *54*, 96–107. [CrossRef]
94. Mirzaie, M.; Darvishzadeh, R.; Shakiba, A.; Matkan, A.A.; Atzberger, C.; Skidmore, A. Comparative Analysis of Different Uni- and Multi-Variate Methods for Estimation of Vegetation Water Content Using Hyper-Spectral Measurements. *Int. J. Appl. Earth Obs. Geoinf.* **2014**, *26*, 1–11. [CrossRef]
95. Yi, Q.; Wang, F.; Bao, A.; Jiapaer, G. Leaf and Canopy Water Content Estimation in Cotton Using Hyperspectral Indices and Radiative Transfer Models. *Int. J. Appl. Earth Obs. Geoinf.* **2014**, *33*, 67–75. [CrossRef]
96. Zhang, L.; Zhou, Z.; Zhang, G.; Meng, Y.; Chen, B.; Wang, Y. Monitoring the Leaf Water Content and Specific Leaf Weight of Cotton (*Gossypium hirsutum* L.) in Saline Soil Using Leaf Spectral Reflectance. *Eur. J. Agron.* **2012**, *41*, 103–117. [CrossRef]

97. Roy, B. Optimum Machine Learning Algorithm Selection for Forecasting Vegetation Indices: MODIS NDVI & EVI. *Remote Sens. Appl.* **2021**, *23*, 100582. [[CrossRef](#)]
98. Qiu, R.; Li, X.; Han, G.; Xiao, J.; Ma, X.; Gong, W. Monitoring Drought Impacts on Crop Productivity of the U.S. Midwest with Solar-Induced Fluorescence: GOSIF Outperforms GOME-2 SIF and MODIS NDVI, EVI, and NIRv. *Agric. For. Meteorol.* **2022**, *323*, 109038. [[CrossRef](#)]
99. Xu, Y.; Chen, Y.; Yang, J.; Zhang, W.; Wang, Y.; Wei, J.; Cheng, W. Drought in Shanxi Province Based on Remote Sensing Drought Index Analysis of Spatial and Temporal Variation Characteristics. *Atmosphere* **2023**, *14*, 799. [[CrossRef](#)]
100. Khalis, H.; Sadiki, A.; Jawhari, F.; Mesrar, H.; Azab, E.; Gobouri, A.A.; Adnan, M.; Bourhia, M. Effects of Climate Change on Vegetation Cover in the Oued Lahdar Watershed. Northeastern Morocco. *Plants* **2021**, *10*, 1624. [[CrossRef](#)]
101. Belmahi, M.; Hanchane, M.; Krakauer, N.Y.; Kessabi, R.; Bouayad, H.; Mahjoub, A.; Zouhri, D. Analysis of Relationship between Grain Yield and NDVI from MODIS in the Fez-Meknes Region, Morocco. *Remote Sens.* **2023**, *15*, 2707. [[CrossRef](#)]
102. Irik, H.A.; Kaymaz, E.; Saban Polu, P.; Beyzi, E.; Varol, İ.S.; Unlukara, A.; Kirnak, H. Potential Use of Crop Water Stress Index (CWSI) and Spectral Vegetation Indices for Black Cumin under Deficit Irrigation. *Environ. Sci. Eur.* **2024**, *36*, 93. [[CrossRef](#)]
103. Idso, S.B.; Jackson, R.D.; Pinter, P.J.; Reginato, R.J.; Hatfield, J.L. Normalizing the Stress-Degree-Day Parameter for Environmental Variability. *Agric. Meteorol.* **1981**, *24*, 45–55. [[CrossRef](#)]
104. Jackson, R.D. Canopy Temperature and Crop Water Stress. In *Advances in Irrigation*; Elsevier: Amsterdam, The Netherlands, 1981; Volume 1, pp. 43–85, ISBN 0275-7915.
105. Çolak, Y.B.; Yazar, A.; Çolak, İ.; Akça, H.; Duraktekin, G. Evaluation of Crop Water Stress Index (CWSI) for Eggplant under Varying Irrigation Regimes Using Surface and Subsurface Drip Systems. *Agric. Agric. Sci. Procedia* **2015**, *4*, 372–382. [[CrossRef](#)]
106. Chen, J.; Lin, L.; Lü, G. An Index of Soil Drought Intensity and Degree: An Application on Corn and a Comparison with CWSI. *Agric. Water Manag.* **2010**, *97*, 865–871. [[CrossRef](#)]
107. Tong, X.; Mu, Y.; Zhang, J.; Meng, P.; Li, J. Water Stress Controls on Carbon Flux and Water Use Efficiency in a Warm-Temperate Mixed Plantation. *J. Hydrol.* **2019**, *571*, 669–678. [[CrossRef](#)]
108. Egea, G.; Padilla-Díaz, C.M.; Martínez-Guanter, J.; Fernández, J.E.; Pérez-Ruiz, M. Assessing a Crop Water Stress Index Derived from Aerial Thermal Imaging and Infrared Thermometry in Super-High Density Olive Orchards. *Agric. Water Manag.* **2017**, *187*, 210–221. [[CrossRef](#)]
109. Gorelick, N.; Hancher, M.; Dixon, M.; Ilyushchenko, S.; Thau, D.; Moore, R. Google Earth Engine: Planetary-Scale Geospatial Analysis for Everyone. *Remote Sens. Environ.* **2017**, *202*, 18–27. [[CrossRef](#)]
110. Tabari, H.; Abghari, H.; Hosseinzadeh Talaei, P. Temporal Trends and Spatial Characteristics of Drought and Rainfall in Arid and Semiarid Regions of Iran. *Hydrol. Process.* **2012**, *26*, 3351–3361. [[CrossRef](#)]
111. Wang, S.; Xing, X.; Wu, Y.; Guo, J.; Li, M.; Fu, B. Seasonal Response of the NDVI to the SPEI at Different Time Scales in Yinshanbeilu, Inner Mongolia, China. *Land* **2024**, *13*, 523. [[CrossRef](#)]
112. Fines, R.W.; Stone, M.; Webster, K.L.; Leach, J.A.; Buttle, J.M.; Emelko, M.B.; Collins, A.L. Evaluation of Legacy Forest Harvesting Impacts on Dominant Stream Water Sources and Implications for Water Quality Using End Member Mixing Analysis. *Water* **2023**, *15*, 2825. [[CrossRef](#)]
113. Langhammer, J.; Su, Y.; Bernsteinová, J. Runoff Response to Climate Warming and Forest Disturbance in a Mid-Mountain Basin. *Water* **2015**, *7*, 3320–3342. [[CrossRef](#)]
114. Aryal, Y.; Zhu, J. Effect of Watershed Disturbance on Seasonal Hydrological Drought: An Improved Double Mass Curve (IDMC) Technique. *J. Hydrol.* **2020**, *585*, 124746. [[CrossRef](#)]

Disclaimer/Publisher’s Note: The statements, opinions and data contained in all publications are solely those of the individual author(s) and contributor(s) and not of MDPI and/or the editor(s). MDPI and/or the editor(s) disclaim responsibility for any injury to people or property resulting from any ideas, methods, instructions or products referred to in the content.